An efficient method for the incompressible Navier-Stokes equations on irregular domains with no-slip boundary conditions, high order up to the boundary.

D. Shirokoff, R. R. Rosales

Department of Mathematics, Massachusetts Institute of Technology, Cambridge, MA, USA, 02139

Abstract

Common efficient schemes for the incompressible Navier-Stokes equations, such as projection or fractional step methods, have limited temporal accuracy as a result of matrix splitting errors, or introduce errors near the domain boundaries (which destroy uniform convergence to the solution). In this paper we recast the incompressible (constant density) Navier-Stokes equations (with the velocity prescribed at the boundary) as an equivalent system, for the primary variables velocity and pressure. We do this in the usual way away from the boundaries, by replacing the incompressibility condition on the velocity by a Poisson equation for the pressure. The key difference from the usual approaches occurs at the boundaries, where we use boundary conditions that unequivocally allow the pressure to be recovered from knowledge of the velocity at any fixed time. This avoids the common difficulty of an, apparently, over-determined Poisson problem. Since in this alternative formulation the pressure can be accurately and efficiently recovered from the velocity, the recast equations are ideal for numerical marching methods. The new system can be discretized using a variety of methods, including semi-implicit treatments of viscosity, and in principle to any desired order of accuracy. In this work we illustrate the approach with a 2-D second order finite difference scheme on a Cartesian grid, and devise an algorithm to solve the equations on domains with curved (non-conforming) boundaries, including a case with a non-trivial topology (a circular obstruction inside the domain).

Email addresses: `shirokof@math.mit.edu` (D. Shirokoff), `rrr@math.mit.edu` (R. R. Rosales)

This algorithm achieves second order accuracy in the L^∞ norm, for both the velocity and the pressure. The scheme has a natural extension to 3-D.

---

1. Introduction.

A critical issue in the numerical solution of the incompressible Navier-Stokes equations is the question of how to implement the incompressibility constraint. Equivalently, how to recover the pressure from the flow velocity, given the fact that the equations do not provide any boundary condition for the pressure. This has been an area of intense research, ever since the pioneering MAC scheme [18] of Harlow and Welch in 1965. Of course, one can avoid the problem by simultaneously discretizing the momentum and the divergence free equations, as in the difference scheme proposed by Krzywicki and Ladyzhenskaya [29], which can be shown to converge — while avoiding the need for any pressure boundary conditions. Approaches such as these, however, do not lead to efficient schemes.

Generally the dilemma has been that of a trade-off between efficiency, and accuracy of the computed solution near the boundary. However, many applications require both efficiency, and accuracy. For example, to calculate fluid solid interactions, both the pressure and gradients of the velocity are needed at the solid walls, as they appear in the components of the stress tensor. Furthermore, these objectives must be achievable for "arbitrary" geometries, not just simple ones with symmetries that can be exploited. Unfortunately, these requirements are not something that current algorithms are generally well suited for, as the brief review below is intended to show.[1] However, we believe that algorithms based on a Presure Poisson Equation (PPE) reformulation of the Navier-Stokes equations — reviewed towards the end of this introduction — offer a path out of the dilemma. The work presented in this paper is, we hope, a contribution in this direction.

Projection methods are very popular in practice because they are efficient. They achieve this efficiency by: (i) Interpreting the pressure as effecting a projection of the flow velocity evolution into the set of incompressible fields.

---

[1]This is not intended as a thorough review of the field, and we apologize for the many omissions.

That is, write the equations in the form $\mathbf{u}_t = \mathcal{P}\left(\mu\,\Delta\,\mathbf{u} - (\mathbf{u}\cdot\nabla)\,\mathbf{u} + \mathbf{f}\right)$, where $\mathcal{P}$ is the appropriate projection operator, μ is the kinematic viscosity, $\mathbf{u}$ is the flow velocity vector, and $\mathbf{f}$ is the vector of applied body forces. (ii) Directly evolving the flow velocity. The question is then how to compute $\mathcal{P}$.

In their original formulation by Chorin [7] and Temam [48], the projection method was formulated as a time splitting scheme in which: First an intermediate velocity is computed, ignoring incompressibility. Second, this velocity is projected onto the space of incompressible vector fields — by solving a Poisson equation for pressure. Unfortunately this process introduces numerical boundary layers into the solution, which can be ameliorated (but not completely suppressed) for simple geometries — e.g. ones for which a staggered grid approach can be implemented [8].

The development of *second order projection methods* [2, 25, 27, 35, 50] provided greater control over the numerical boundary layers and accuracy in the pressure [4]. These are the most popular schemes used in practice. However, particularly for moderate or low Reynolds numbers, the effects of the numerical boundary layers can still be problematic [16]. Non-conforming boundaries add an extra layer of difficulty. The search for means to better control these numerical artifacts is an active area of research.

The numerical boundary layers in projection methods reflect in the known convergence results for them (e.g. [40, 42, 45]). Convergence is stated only in terms of integral norms, with the main difficulties near the boundary. There point-wise convergence (and even less convergence of the flow velocity gradient) cannot be guaranteed — even if the solution is known to be smooth. Hence the accurate calculation of wall stresses with these methods is problematic. Guermond, Minev and Shen [16] provide further details on convergence results, as well as an extensive review of projection methods and the improved pressure-correction schemes.

Two other methods for solving the Navier-Stokes equations are the *immersed boundary* [31, 33, 37, 38, 47], and the *vortex-streamfunction* [3, 5, 34] methods. These also decouple the calculation of the velocity and of the pressure. The immersed boundary method does so by introducing Dirac forces to replace the domain walls, which makes obtaining high order implementation of the boundary conditions difficult. The vortex-streamfunction formulation decouples the equations, but has dimensional limitations. An interesting variation of the vortex-streamfunction approach, using only local boundary conditions, is presented in reference [17].

Closely related to the immersed boundary methods are the *penalty* (alter-

natively: *fictitious domain* or *domain embedding*) methods — e.g. see [1, 11, 26]. These methods, effectively, replace solid walls in the fluid by a porous media with a small porosity $0 < \eta \ll 1$. In the limit $\eta \to 0$, this yields no slip and no flow-through at the solid walls. Two important advantages of this approach are that complicated domains are easy to implement, and that the total fluid-solid force can be computed using a volume integral, rather than an integral over the boundary of the solid. Unfortunately, the parameter η introduces $\sqrt{\eta}$ boundary layers which make convergence slow and high accuracy computations expensive, since η cannot be selected independently of the numerical grid size.

Finally, we mention the algorithms based on a *Pressure Poisson Equation (PPE) reformulation of the Navier-Stokes equations* [19, 20, 21, 32, 15, 23, 24, 28, 41, 43, 44], which is the class of methods within which the work presented in this paper falls. In this approach the incompressibility constraint for the flow velocity is replaced by a Poisson[2] equation for the pressure. This then allows an extra boundary condition — which must be selected so that, in fact, incompressibility is maintained by the resulting system. This strategy was first proposed by Gresho and Sani [15], who pointed out that adding $\nabla \cdot \mathbf{u} = 0$ as a boundary condition yields a system of equations that is equivalent to the Navier-Stokes equations. Unfortunately, their particular PPE formulation incorporates no explicit boundary condition that can be used to recover the pressure from the velocity, by solving a Poisson problem — for a more detailed discussion of this, see remark 4 in this paper. In [19, 20] the issue is resolved at the discrete numerical level, where they demonstrate high order schemes. For instance [19] demonstrates a fourth-order in space and 2nd-order in time implementation using overlapping grids. Subsequent work at the continuum level was later introduced by Henshaw et. al. [21] and Johnston and Liu [24]. Recently, work in PPE formulations have led to interesting improvements and analysis of projection methods [32]. In this paper — in equations (20–21) — we present another PPE system, also equivalent to the Navier-Stokes equations, which allows an explicit recovery of the pressure given the flow velocity. A comparison with the one in [24] can be found in remark 5 in this paper. Subtle issues can arise with semi-implicit approaches (pressure treated explicitly and viscous term implicitly) leading to time step restrictions [39]. In section 5 we show that semi-implicit

---

[2]The choice of the Poisson equation for the pressure is not unique, e.g. see [23].

implementations of our scheme do not have time step restrictions of the diffusive type.

PPE reformulations of the Navier-Stokes equations, such as the one in equations (20–21), or in reference [24], have important advantages over the standard form of the equations. First, the pressure is not implicitly coupled to the velocity through the momentum equation and incompressibility. Hence it can be directly (and efficiently) recovered from the velocity field by solving a Poisson equation. This allows the velocity field to be marched in time using the momentum equation, with the pressure interpreted as some (complicated) function of the velocity. Second, no spurious boundary layers are generated for neither the velocity, nor the pressure. This because:

— There are no ambiguities as to which boundary conditions to use for the pressure — hence errors induced by not-quite-correct boundary conditions do not occur. Note that these errors should not be confused with the truncation errors that any discretization of the equations will produce. Truncation errors are controlled by the order of the approximation and, for smooth solutions, are uniformly small.

— Incompressibility is enforced at all times.

Hence pressure and velocities that are accurate everywhere can be obtained, in particular: near the boundaries. Finally, PPE formulations allow, at least in principle, for the systematic generation of higher order approximations.

It follows that PPE strategies offer the promise of a resolution of the dilemma alluded to in the second paragraph of this introduction. They retain many of the advantages that have made projection methods popular, while not suffering from the presence of numerical boundary layers. On the negative side, the boundary conditions for PPE systems tend to be more complicated than the simple ones that the standard form of the equations has.

This paper is organized as follows. In § 2 we discuss the Pressure Poisson Equation (PPE) formulation of the Navier-Stokes equations. In § 3 we present a PPE formulation, using an alternative form of the boundary conditions, that allows a complete splitting of the momentum and pressure equations. Namely: the pressure can be recovered from the flow velocity without boundary condition ambiguities. In § 4 we address a numerical question (secular growth of the error under some conditions) and introduce a corrected formulation, involving a feedback parameter λ, where this potential problem is corrected. This system, which is equivalent to the Navier-Stokes equations, is displayed in equations (20–21). A discussion and comparison with

the alternative PPE formulation by Johnston and Liu [24] is also included in this section. In § 5 we introduce and examine a second order in time, semi-implicit in viscosity scheme. We show the scheme is unconditionally stable with no diffusive time step restriction. In § 6 we describe a second order solver for the new system introduced in § 4, for irregular domains embedded within a cartesian staggered grid. In § 7, we implement and test our proposed schemes. This section includes convergence plots, indicating *second order uniform convergence* all the way to the boundary (L^∞ norm), *of the pressure, the flow velocity, and of the derivatives of the flow velocity.* Finally, § 8 has the conclusions. The contents of the two appendices is as follows. In Appendix A we present an extended system of equations, valid for arbitrary flows, which for smooth solutions has the Navier-Stokes equations as an attractor. In Appendix B, for completeness, we display formulas for the $\nabla \cdot \mathbf{u} = 0$ boundary condition for general conforming boundaries in curvilinear coordinates.

2. The Pressure Poisson Equation.

In this section we introduce the well-known pressure Poisson equation (PPE), and use it to construct a system of equations (and boundary conditions) equivalent to the constant-density (hence incompressible) Navier-Stokes equations, with the velocity prescribed at the boundaries. Specifically, consider the incompressible Navier-Stokes equations in a connected domain $\Omega \in \mathbb{R}^D$, where $D = 2$ or $D = 3$, with a piece-wise smooth boundary $\partial\Omega$. Inside Ω, the flow velocity field $\mathbf{u}(\mathbf{x}, t)$ satisfies the equations

$$\mathbf{u}_t + (\mathbf{u} \cdot \nabla)\,\mathbf{u} \;=\; \mu\,\Delta\mathbf{u} - \nabla p + \mathbf{f}, \tag{1}$$
$$\nabla \cdot \mathbf{u} \;=\; 0, \tag{2}$$

where μ is the kinematic viscosity,[3] $p(\mathbf{x}, t)$ is the pressure, $\mathbf{f}(\mathbf{x}, t)$ are the body forces, ∇ is the gradient, and $\Delta = \nabla^2$ is the Laplacian. Equation (1) follows from the conservation of momentum, while (2) is the incompressibility condition (conservation of mass).

In addition, the following boundary conditions apply

$$\mathbf{u} = \mathbf{g}(\mathbf{x}, t) \qquad \text{for } \mathbf{x} \in \partial\Omega, \tag{3}$$

---

[3]We work in non-dimensional variables, so that $\mu = 1/Re$ (where Re is the Reynolds number) and the fluid density is $\rho = 1$.

where

$$\int_{\partial\Omega} \mathbf{n} \cdot \mathbf{g} \, \mathrm{d}A = 0, \tag{4}$$

$\mathbf{n}$ is the outward unit normal on the boundary, and $\mathrm{d}A$ is the area (length in 2D) element on $\partial\Omega$. Equation (4) is the consistency condition for $\mathbf{g}$, since an incompressible fluid must have zero net flux through the boundary.

Finally, we assume that initial conditions are given

$$
\begin{aligned}
\mathbf{u}(\mathbf{x}, 0) &= \mathbf{u}_0 & \text{for } \mathbf{x} \in \Omega, & \tag{5} \\
\nabla \cdot \mathbf{u}_0 &= 0 & \text{for } \mathbf{x} \in \Omega, & \tag{6} \\
\mathbf{u}_0(\mathbf{x}) &= \mathbf{g}(\mathbf{x}, 0) & \text{for } \mathbf{x} \in \partial\Omega. & \tag{7}
\end{aligned}
$$

Remark 1. Of particular interest is the case of fixed impermeable walls, where no flux $\mathbf{u} \cdot \mathbf{n} = 0$ and no slip $\mathbf{u} \times \mathbf{n} = 0$ apply at $\partial\Omega$. This corresponds to $\mathbf{g} = 0$ in (3). Note that the no-slip condition is equivalent to $\mathbf{u} \cdot \mathbf{t} = 0$ for all unit tangent vectors $\mathbf{t}$ to the boundary. ♣

Remark 2. In this paper we will assume that the domain Ω is fixed. Situations where the boundary of the domain, $\partial\Omega$, can move — either by externally prescribed factors, or from interactions with the fluid, are of great physical interest. However, to keep the presentation of the new method as simple as possible, we postpone consideration of these cases for further work. ♣

Next we introduce the Pressure Poisson Equation (PPE). To obtain the pressure equation, take the divergence of the momentum equation (1), and apply equation (2) to eliminate the viscous term and the term with a time derivative. This yields the following Poisson equation for the pressure

$$\Delta p = \nabla \cdot (\mathbf{f} - (\mathbf{u} \cdot \nabla) \mathbf{u}) . \tag{8}$$

Two crucial questions are now (for simplicity, *assume solutions that are smooth all the way up to the boundary*)

2a *Can this equation be used to replace the incompressibility condition (2)?*
Since — given (8) — the divergence of (1) yields the heat equation

$$\phi_t = \mu \Delta \phi, \tag{9}$$

for $\phi = \nabla \cdot \mathbf{u}$ and $\mathbf{x} \in \Omega$, it would seem that the answer to this question is yes — provided that the initial conditions are incompressible (*i.e.*: $\phi = 0$ for $t = 0$). However, this works only if we can guarantee that, at all times,

$$\phi = 0, \tag{10}$$

for $\mathbf{x} \in \partial\Omega$.

2b *Given the flow velocity* $\mathbf{u}$, *can (8) be used to obtain the pressure p?* Again, at first sight, the answer to this question appears to be yes. After all, (8) is a Poisson equation for p, which should determine it uniquely — given appropriate boundary conditions. The problem is: what boundary conditions? Evaluation of (1) at the boundary, with use of (3), shows that the flow velocity determines the whole gradient of the pressure at the boundary, which is too much for (8). Further, if only a portion of these boundary conditions are enforced when solving (8) — say, the normal component of (1) at the boundary, then how can one be sure that the whole of (1) applies at the boundary?

Remark 3. From an algorithmic point of view, an affirmative answer to the questions above would very useful, for then one could think of the pressure as some (global) function of the flow velocity, in which case (1) becomes an evolution equation for $\mathbf{u}$, which could then be solved with a numerical "marching" method. ♣

The issue in item 2a can be resolved easily, and we do so next. We postpone dealing with the issue in item 2b till the next section, § 3. Since the addition of an equation for the pressure allows the introduction of one extra boundary condition, we propose to replace the system in (1), (2), and (3) by the following Pressure Poisson Equation (PPE) formulation:

$$\mathbf{u}_t + (\mathbf{u} \cdot \nabla)\mathbf{u} = \mu\,\Delta\mathbf{u} - \nabla p + \mathbf{f}, \tag{11}$$
$$\Delta p = \nabla \cdot (\mathbf{f} - (\mathbf{u} \cdot \nabla)\mathbf{u}), \tag{12}$$

for $\mathbf{x} \in \Omega$, with the boundary conditions

$$\mathbf{u} = \mathbf{g}(\mathbf{x},\,t), \tag{13}$$
$$\nabla \cdot \mathbf{u} = 0, \tag{14}$$

for $\mathbf{x} \in \partial\Omega$ — where, of course, the restriction in (4) still applies. The extra boundary condition is precisely what is needed to ensure that the pressure enforces incompressibility throughout the flow (see item 2a)

8

Remark 4. It can be seen that for smooth enough solutions $(\mathbf{u}, p)$, the pair of equations (11–12), accompanied by the boundary conditions (13–14), are equivalent to the incompressible Navier-Stokes equations in (1), (2), and (3). Of course, this result is not new. This reformulation of the Navier-Stokes equations was first presented by Gresho and Sani [15] — it can also be found in reference [41]. However, it should be pointed out that Harlow and Welch [18], in their pioneering work, had already noticed that the boundary condition $\nabla \cdot \mathbf{u} = 0$ was needed to guarantee, within the context of their MAC scheme, that $\nabla \cdot \mathbf{u} = 0$ everywhere.

This formulation does not provide any boundary conditions for the pressure, which means that one ends up with a "global" constraint on the solutions to the Poisson equation (12). Hence it does not yield a satisfactory answer to the issue in item 2b, since recovering the pressure from the flow velocity is a hard problem with this approach.

Direct implementations of (11–14) have only been proposed for simple geometries — in particular: grid-conforming boundaries. In [28] a spectral algorithm for plane channel flows is presented. We have already mentioned [18], where they use a staggered grid on a rectangular domain, and the condition $\nabla \cdot \mathbf{u} = 0$ is used (at the discrete level) to close the linear system for the pressure. In [23], by manipulating the discretization of the boundary conditions and of the momentum equation (11), they manage to obtain "local" approximate Neumann conditions for the pressure — both on rectangular, as well as circular, domains where $\mathbf{u} = 0$ on the boundary. Unfortunately, the approaches in [18, 23] seem to be very tied up to the details of particular discretizations, and require a conforming boundary. ♣

3. Theoretical Reformulation

We still need to deal with the issue raised in item 2b. In particular, in order to implement the ideas in remark 3, we need to split the boundary conditions for (11–12), in such a way that: (i) there is a specific part of the boundary conditions that is used with (11) to advance the velocity field in time, given the pressure. (ii) The remainder of the boundary conditions is used with (12) to solve for the pressure — at each fixed time, given the flow velocity field $\mathbf{u}$. This is the objective of this section.

The conventional approach in projection or fractional step methods is to associate (13) with equation (11). This is reasonable for evolving the heat-like equation (11). Unfortunately, it has the drawback of only implicitly

defining the boundary conditions for the Poisson equation (12). Specifically, the correct pressure boundary conditions are those that guarantee $\nabla \cdot \mathbf{u} = 0$ for $\mathbf{x} \in \partial\Omega$, and such boundary conditions cannot easily be known a priori as a function of $\mathbf{u}$. Hence one is left with a situation where the appropriate boundary conditions for the pressure are not known. This leads to errors in the pressure, and in the incompressibility condition, which are difficult to control. In particular, errors are often most pronounced near the boundary where no local error estimates can be produced, even for smooth solutions. By the latter we mean that the resulting schemes cannot be shown to be consistent, all the way up to the boundary, in the classical sense of finite differences introduced by Lax [30].

In this paper we take a different approach, which has a similar spirit to the one used by Johnston and Liu [24] — see remark 5. Rather than associate all the D components of (13) with equation (11), we enforce the $D - 1$ tangential components only, and complete the set of boundary conditions for (11) with (14). Hence, when evolving equation (11) we do not specify the normal velocity on the boundary, but — through the divergence condition (14) — specify the normal derivative of the normal velocity. Finally, the (as yet unused) boundary condition on the normal velocity, $\mathbf{n} \cdot (\mathbf{u} - \mathbf{g}) = 0$ for $\mathbf{x} \in \partial\Omega$, is employed to obtain an explicit boundary condition for equation (12). We do this by requiring that the pressure boundary condition be equivalent to $(\mathbf{n} \cdot (\mathbf{u} - \mathbf{g}))_t = 0$ for $\mathbf{x} \in \partial\Omega$ — which then guarantees that the normal component of (13) holds, as long as the initial conditions satisfy it. This objective is easily achieved: dotting equation (11) through with $\mathbf{n}$, and evaluating at the boundary yields the desired condition. The equations, with their appropriate boundary conditions, are thus:

$$\left.\begin{aligned} \mathbf{u}_t - \mu\,\Delta\mathbf{u} &= -\nabla p - (\mathbf{u} \cdot \nabla)\,\mathbf{u} + \mathbf{f} && \text{for } \mathbf{x} \in \ \Omega, \\ \mathbf{n} \times (\mathbf{u} - \mathbf{g}) &= 0 && \text{for } \mathbf{x} \in \partial\Omega, \\ \nabla \cdot \mathbf{u} &= 0 && \text{for } \mathbf{x} \in \partial\Omega, \end{aligned}\right\} \quad (15)$$

and

$$\left.\begin{aligned} \Delta p &= -\nabla \cdot ((\mathbf{u} \cdot \nabla)\,\mathbf{u}) + \nabla \cdot \mathbf{f} && \text{for } \mathbf{x} \in \ \Omega, \\ \mathbf{n} \cdot \nabla p &= \mathbf{n} \cdot (\mathbf{f} - \mathbf{g}_t + \mu\,\Delta\mathbf{u} - (\mathbf{u} \cdot \nabla)\,\mathbf{u}) && \text{for } \mathbf{x} \in \partial\Omega. \end{aligned}\right\} \quad (16)$$

Again, for smooth (up to the boundary) enough solutions $(\mathbf{u},\, p)$ of the equations: the incompressible Navier-Stokes equations (1–2), with boundary conditions as in (3), are equivalent to the system of equations and boundary conditions in (15–16).

For the sake of completeness, we display now the calculation showing that the boundary condition splitting in (15–16) recovers the normal velocity boundary condition $\mathbf{n} \cdot \mathbf{u} = \mathbf{n} \cdot \mathbf{g}$. To start, dot the first equation in (15) with the normal $\mathbf{n}$, and evaluate at the boundary. This yields

$$\mathbf{n} \cdot \mathbf{u}_t = \mathbf{n} \cdot (\mu \, \Delta \mathbf{u} - \nabla p - (\mathbf{u} \cdot \nabla) \, \mathbf{u} + \mathbf{f}) \quad \text{for } \mathbf{x} \in \partial \Omega. \qquad (17)$$

Next, eliminate $\mathbf{n} \cdot \nabla p$ from this last equation — by using the boundary condition for the pressure in (16), to obtain

$$(\mathbf{n} \cdot (\mathbf{u} - \mathbf{g}))_t = 0 \quad \text{for } \mathbf{x} \in \partial \Omega. \qquad (18)$$

This is a trivial ODE for the normal component of the velocity at each point in the boundary. Thus, provided that $\mathbf{n} \cdot (\mathbf{u} - \mathbf{g}) = 0$ initially, it holds for all time.

An important final point to check is the solvability condition for the pressure problem. Given the flow velocity $\mathbf{u}$ at time t, equation (16) is a Poisson problem with Neumann boundary conditions for the pressure. This problem has a solution (unique up to an additive constant) if and only if the "flux equals source" criteria

$$\int_{\partial \Omega} \mathbf{n} \cdot (\mathbf{f} - \mathbf{g}_t + \mu \, \Delta \mathbf{u} - (\mathbf{u} \cdot \nabla) \, \mathbf{u}) \, \mathrm{d}A = \int_{\Omega} \nabla \cdot (\mathbf{f} - (\mathbf{u} \cdot \nabla) \, \mathbf{u}) \, \mathrm{d}V \qquad (19)$$

applies. This is satisfied because:

3a $\int_{\partial \Omega} \mathbf{n} \cdot (\mathbf{f} - (\mathbf{u} \cdot \nabla) \, \mathbf{u}) \, \mathrm{d}A = \int_{\Omega} \nabla \cdot (\mathbf{f} - (\mathbf{u} \cdot \nabla) \, \mathbf{u}) \, \mathrm{d}V$,

3b $\int_{\partial \Omega} \mathbf{n} \cdot \Delta \mathbf{u} \, \mathrm{d}A = \int_{\Omega} \Delta \, (\nabla \cdot \mathbf{u}) \, \mathrm{d}V = 0$,

3c $\int_{\partial \Omega} \mathbf{n} \cdot \mathbf{g}_t \, \mathrm{d}A = \frac{\partial}{\partial t} \int_{\partial \Omega} \mathbf{n} \cdot \mathbf{g} \, \mathrm{d}A = 0$,

where we have used Gauss' theorem, incompressibility, and (4).

4. Modification for Stability

For the system of equations in (15–16), it is important to notice that

4a The tangential boundary condition on the flow velocity, $\mathbf{n} \times (\mathbf{u} - \mathbf{g}) = 0$ for $\mathbf{x} \in \partial \Omega$, is enforced explicitly.

4b The incompressibility condition, $\nabla \cdot \mathbf{u} = 0$ for $\mathbf{x} \in \Omega$, is enforced "exponentially". By this we mean that any errors in satisfying the incompressibility condition are rapidly damped, because $\phi = \nabla \cdot \mathbf{u}$ satisfies (9–10). Thus this condition is enforced in a robust way, and we do not expect it to cause any trouble for "reasonable" numerical discretizations of the equations.

4c By contrast, the normal boundary condition on the flow velocity, $\mathbf{n} \cdot (\mathbf{u} - \mathbf{g}) = 0$ for $\mathbf{x} \in \partial\Omega$, is enforced in a rather weak fashion. By this we mean that errors in satisfying this condition are not damped at all by equation (18). Thus, this condition lacks the inherent stability provided by the heat equation. In practice, numerical errors add (effectively) noise to equation (18), resulting in a drift of the normal velocity component. This can have de-stabilizing effects on the behavior of a numerical scheme. Hence it is a problem that must be corrected.

In this section we alter the PPE equations (15–16) to address the problem pointed out in item 4c. We do this by adding an appropriate "stabilizing" term. The idea is similar in nature to the feedback controller introduced in [12] for immersed boundary methods. Our goal here is to develop a pair of differential equations — fully equivalent to (15–16) — which are suitable for numerical implementation. In order to resolve the issue in item 4c, we add a feedback term to the equations, by altering the pressure boundary condition. Specifically, we modify the equations from (15–16) to

$$
\left.
\begin{aligned}
\mathbf{u}_t - \mu\,\Delta\mathbf{u} &= -\nabla p - (\mathbf{u} \cdot \nabla)\,\mathbf{u} + \mathbf{f} && \text{for } \mathbf{x} \in \ \Omega, \\
\mathbf{n} \times (\mathbf{u} - \mathbf{g}) &= 0 && \text{for } \mathbf{x} \in \partial\Omega, \\
\nabla \cdot \mathbf{u} &= 0 && \text{for } \mathbf{x} \in \partial\Omega,
\end{aligned}
\right\}
\qquad (20)
$$

and

$$
\left.
\begin{aligned}
\Delta p &= -\nabla \cdot ((\mathbf{u} \cdot \nabla)\,\mathbf{u}) + \nabla \cdot \mathbf{f} && \text{for } \mathbf{x} \in \ \Omega, \\
\mathbf{n} \cdot \nabla p &= \mathbf{n} \cdot (\mathbf{f} - \mathbf{g}_t + \mu\,\Delta\mathbf{u} - (\mathbf{u} \cdot \nabla)\,\mathbf{u}) \\
&+ \ \lambda\,\mathbf{n} \cdot (\mathbf{u} - \mathbf{g}) && \text{for } \mathbf{x} \in \partial\Omega,
\end{aligned}
\right\}
\qquad (21)
$$

where $\lambda > 0$ is a numerical parameter — see § 4.1. This system is still equivalent to the incompressible Navier-Stokes equations and boundary conditions in (1–3), for smooth (up to the boundary) enough solutions $(\mathbf{u}, p)$.

12

The heat equation (9–10) for $\phi = \nabla \cdot \mathbf{u}$ still applies, while the equation for the evolution of the normal velocity at the boundary changes from (18) to:

$$(\mathbf{n} \cdot (\mathbf{u} - \mathbf{g}))_t = -\lambda \, \mathbf{n} \cdot (\mathbf{u} - \mathbf{g}) \quad \text{for } \mathbf{x} \in \partial\Omega. \tag{22}$$

Thus, if $\mathbf{n} \cdot (\mathbf{u} - \mathbf{g}) = 0$ initially, it remains so for all times. In addition, this last equation shows that this new system resolves the issue pointed out in item 4c.

Finally, we check what happens to the solvability condition for the pressure problem, given the system change above. Clearly, all we need to do is to modify equation (19) by adding — to its left hand side, the term

$$\lambda \int_{\partial\Omega} \mathbf{n} \cdot (\mathbf{u} - \mathbf{g}) \ \mathrm{d}A = \lambda \int_{\Omega} \nabla \cdot \mathbf{u} \ \mathrm{d}V - \lambda \int_{\partial\Omega} \mathbf{n} \cdot \mathbf{g} \ \mathrm{d}A = 0, \tag{23}$$

where we have used incompressibility, and equation (4). It follows that solvability remains valid.

Remark 5. The reformulation of the Navier-Stokes equations in (20–21) is similar to the one used by Johnston and Liu in [24]. In their paper the authors propose methods of solution to the Navier-Stokes equations based on the equivalent system (for simplicity, we set $\mathbf{g} = 0$, as done in [24]) where

(a) For $\mathbf{x} \in \ \Omega$, the same equations as in (20–21) apply.

(b) For $\mathbf{x} \in \partial\Omega$, $\mathbf{u} = 0$ is used for the momentum equation.

(c) For $\mathbf{x} \in \partial\Omega$, $\mathbf{n} \cdot \nabla p = \mathbf{n} \cdot (-\mu \, \nabla \times \nabla \times \mathbf{u} + \mathbf{f})$ is used for the Poisson equation.

For this system the incompressibility condition $\phi = \nabla \cdot \mathbf{u} = 0$ follows because these equations yield

(d) $\phi_t = \mu \, \Delta \, \phi$ for $\mathbf{x} \in \Omega$, with $\mathbf{n} \cdot \nabla \, \phi = 0$ for $\mathbf{x} \in \partial\Omega$.

Thus, if ϕ vanishes initially, it will vanish for all times.

(e) The *main advantage* of this reformulation over the one in (20–21) is that (in general) the boundary condition $\nabla \cdot \mathbf{u} = 0$ in (20) may couple the components of the flow velocity field — see § 6.3. Thus, depending on implementation, an implicit treatment of the viscous terms in (20–21) may be more expensive (and complicated) than for the system in items a–c above. However, it is not clear to us at this moment how

13

much of a problem this is. The reason is that the coupling is "weak", by which we mean that: in the $N_G \times N_G$ discretization matrix for the Laplacian — where N_G is the number of points in the numerical grid, the coupling induced by the boundary condition affects only $O(N_G^{1/2})$ entries in 2-D, and $O(N_G^{1/3})$ entries in 3-D — at least with the type of discretization that we use in § 6.3. Hence, it may be possible to design algorithms where the extra cost is moderate, and not a show-stopper.

(f) In cases where the viscosity μ is small, the velocity divergence ϕ may not be adequately damped by the heat equation. It is possible [19, 21] to modify the method by adding a parameter that forces an exponential decay of ϕ to zero. For example: modify the Poisson equation for the pressure to

$$\Delta p = -\nabla \cdot ((\mathbf{u} \cdot \nabla) \mathbf{u}) + \nabla \cdot \mathbf{f} + \lambda \nabla \cdot \mathbf{u}.$$

This then changes the system in item d to

$$\phi_t = \mu \, \Delta \, \phi - \lambda \, \phi \ \text{ for } \ \mathbf{x} \in \Omega, \ \text{ with } \ \mathbf{n} \cdot \nabla \, \phi = 0 \ \text{ for } \ \mathbf{x} \in \partial \Omega.$$

♣

Remark 6. It would be nice to be able to use $\lambda = \lambda(\mathbf{x})$, so as to optimize the implementation of the condition $\mathbf{n} \cdot \mathbf{u} = \mathbf{n} \cdot \mathbf{g}$ for different points along $\partial \Omega$. However, this is not a trivial extension, since it destroys the solvability condition for the pressure. Thus, other (compensating) corrections are needed as well. We postpone the study of this issue for future work. ♣

Remark 7. As show earlier in (19) and (23), the validity of the solvability condition, for the problem in (21), relies on the velocity field satisfying the incompressibility constraint $\nabla \cdot \mathbf{u} = 0$. On the other hand, in the course of a numerical calculation, one may not always start with a numerically divergence free velocity field. This consideration motivates the following theoretical question: *can the equations in (20–21) be modified, so they make sense even for $\nabla \cdot \mathbf{u} \neq 0$?* In Appendix A we show that this is possible. ♣

Remark 8. The contribution from the nonlinear advection term to the right hand side of equation (21) involves second derivatives of the velocity field. For some numerical implementations, such as finite element methods, there

14

are advantages to reducing the number of derivatives in the Poisson equation source terms. For example, reducing the number of derivatives allows one to choose a finite element basis with less regularity. As noted by [24, 19], one may rewrite the nonlinear terms to contain one derivative

$$\left.\begin{aligned}
\Delta p &= \tfrac{1}{2}(\nabla \cdot \mathbf{u})^2 - (\nabla \mathbf{u}):(\nabla \mathbf{u})^T + \nabla \cdot \mathbf{f} &&\text{for } \mathbf{x} \in \ \Omega, \\
\mathbf{n} \cdot \nabla p &= \mathbf{n} \cdot (\mathbf{f} - \mathbf{g}_t + \mu \, \Delta \mathbf{u} - (\mathbf{u} \cdot \nabla) \, \mathbf{u}) \\
&+ \ \lambda \, \mathbf{n} \cdot (\mathbf{u} - \mathbf{g}) &&\text{for } \mathbf{x} \in \partial\Omega,
\end{aligned}\right\} \quad (24)$$

By a similar calculation to the one in the appendix of [24], we can show that the pressure equation (24) is equivalent to Navier-Stokes for smooth enough solutions.

4.1. Selection of the parameter λ.

For numerical purposes, here we address the issue of how large λ should be, by using a simple model for the flow's normal velocity drift. Notice that no precision is needed for this calculation, just order of magnitude. In actual practice, one can monitor how well the normal velocity satisfies the boundary condition, and increase λ if needed. In principle one should be wary of using large values for λ, since this will yield stiff behavior in time. However, the calculation below shows that λ does not need to be very large, and does not depend on the grid size Δx.

It seems reasonable to assume that one can model how the numerical errors affect the ODE (22) for $\mathcal{E} = \mathbf{n} \cdot (\mathbf{u} - \mathbf{g})$, by perturbing the coefficients of the equation, and adding a forcing term to it. Hence we modify equation (22) as follows

$$\mathcal{E}_t = -\lambda \, c_p \, \mathcal{E} + \epsilon \, \gamma \quad \text{for } \mathbf{x} \in \partial\Omega, \tag{25}$$

where $\epsilon \ll 1$ characterizes the size of the errors (determined by the order of the numerical method), while $c_p = c_p(\mathbf{x}, t) = 1 + O(\epsilon)$ and $\gamma = \gamma(\mathbf{x}, t) = O(1)$ are functions encoding the numerical errors. What exactly they are depends on the details of the numerical discretization, but for this calculation we do not need to know these details. All we need is that[4]

$$0 < C_M \leq c_p \quad \text{and} \quad |\gamma| \leq \Gamma, \tag{26}$$

---

[4]For smooth enough solutions, where the truncation errors are controlled by some derivative of the solution.

where C_M and Γ are some positive constants, with $C_M \approx 1$, and $\Gamma = O(1)$ — but not necessarily close to one.

The solution to (25) is given by

$$\mathcal{E} = \mathcal{E}_0\, e^{-\lambda I_1} + \epsilon \underbrace{\int_0^t \gamma(\mathbf{x},\, s)\, e^{-\lambda I_2}\, \mathrm{d}s}_{J}, \qquad (27)$$

where $\mathcal{E}_0$ is the initial value, $I_1 = I_1(\mathbf{x},\, t) = \int_0^t c_p(\mathbf{x},\, s)\, \mathrm{d}s$, and $I_2 = I_1(\mathbf{x},\, t) - I_1(\mathbf{x},\, s)$. The crucial term is J, since the first term decreases in size, and starts at the initial value. However

$$|J| \leq \Gamma \int_0^t e^{-\lambda C_M\,(t-s)}\, \mathrm{d}s \leq \frac{\Gamma}{\lambda\, C_M}. \qquad (28)$$

Within the framework of a numerical scheme, the normal boundary velocity may deviate from the prescribed velocity by some acceptable error δ. Thus we require $\epsilon\, J = O(\delta)$ or less, which — given (28) — will be satisfied if

$$\lambda \sim \frac{\epsilon\, \Gamma}{\delta\, C_M} \approx \frac{\epsilon\, \Gamma}{\delta}, \quad \text{or larger.} \qquad (29)$$

For the second order numerical scheme in § 6, it is reasonable to expect that $\epsilon = (\Delta x)^2$, and to require that $\delta = (\Delta x)^2$. Then (29) reduces to $\lambda \geq \Gamma$. Of course, we do not know (a priori) what Γ is; this is something that we need to find by numerical experimentation — see the first paragraph in this § 4.1. For the numerical calculations reported in § 7, we found that values in the range $10 \leq \lambda \leq 100$ gave good results.

For this scheme, comparing the time step restriction imposed by feedback $(\Delta t_\lambda < O(1/\lambda))$ to the one imposed by diffusion $\Delta t_\mu < O((\Delta x)^2/\mu)$, results in a stiffness ratio that scales as

$$\frac{\Delta t_\mu}{\Delta t_\lambda} \sim \frac{\lambda}{\mu}\Delta x^2. \qquad (30)$$

Hence for low to moderate Reynolds numbers, λ can be choosen quite large without effecting the stiffness.

5. Stability of Semi-implicit Schemes

In the case of moderate to low Reynolds number flows, the stiff viscosity term $\mu \Delta \mathbf{u}$ requires very small time steps when treated explicitly. Hence,

16

there is a large practical interest in treating $\mu\Delta\mathbf{u}$ implicitly while keeping the associated pressure explicit. In this section we write down and analyze semi-implicit schemes for the PPE splitting (15–16). Inspired by many of the ideas from [24], we then show the subsequent schemes are unconditionally stable.

To analyze the stability of the semi-implicit schemes, we require several properties of the Hodge-Helmholtz decomposition. Given $\mathbf{w} \in L^2$, then $\mathbf{w}$ has a unique orthogonal decomposition as

$$\mathbf{w} = \mathbf{a} + \nabla b, \tag{31}$$

where b is determined by $\Delta b = \nabla \cdot \mathbf{w}$ with boundary conditions $\mathbf{n} \cdot \nabla b = \mathbf{n} \cdot \mathbf{w}$. Hence $\mathbf{a}$ is divergence free with zero normal boundary component. Moreover the component $\mathbf{a}$ is orthogonal in the L^2 norm to every gradient field (i.e., $\langle \mathbf{a}, \nabla \phi \rangle = \int_\Omega \mathbf{a} \cdot \nabla \phi \, dV = 0$ is the standard inner product on $L^2(\Omega)$). We may therefore write $\nabla b = \mathcal{Q}\mathbf{w}$ and $\mathbf{a} = \mathcal{P}\mathbf{w}$ where $\mathcal{P}$ and $\mathcal{Q}$ are complementary orthogonal projections (ie. $\mathcal{P} + \mathcal{Q} = \mathcal{I}$, $\mathcal{P}^2 = \mathcal{P}$ and $\mathcal{P} = \mathcal{P}^\dagger$). As a result, the following identities hold for any vector fields $\mathbf{w}$ and $\mathbf{v}$

$$\begin{align} \langle \mathbf{w}, \mathcal{P}\mathbf{v} \rangle &= \langle \mathcal{P}\mathbf{w}, \mathcal{P}\mathbf{v} \rangle \tag{32} \\ &= \langle \mathcal{P}\mathbf{w}, \mathbf{v} \rangle, \tag{33} \end{align}$$

and

$$\langle \mathbf{w}, \mathbf{w} \rangle = \langle \mathcal{P}\mathbf{w}, \mathcal{P}\mathbf{w} \rangle + \langle \mathcal{Q}\mathbf{w}, \mathcal{Q}\mathbf{w} \rangle. \tag{34}$$

To motivate the stability proofs for semi-implicit time discretizations, note that the linear Navier-Stokes equations can also be written in an equivalent projection form

$$\left. \begin{array}{rcll} \mathbf{u}_t &=& \mu\mathcal{P}\Delta\mathbf{u} & \text{for } \mathbf{x} \in \Omega, \\ \mathbf{n} \times \mathbf{u} &=& 0 & \text{for } \mathbf{x} \in \partial\Omega, \end{array} \right\} \tag{35}$$

Dotting equation (35) through by[5] $-\Delta\mathbf{u} = \nabla \times \nabla \times \mathbf{u} - \nabla(\nabla \cdot \mathbf{u})$ and integrating yields

$$\frac{1}{2}\frac{\partial}{\partial t}\Big(\langle \nabla \times \mathbf{u}, \nabla \times \mathbf{u} \rangle + \langle \nabla \cdot \mathbf{u}, \nabla \cdot \mathbf{u} \rangle\Big) = -\mu\langle \Delta\mathbf{u}, \mathcal{P}\Delta\mathbf{u} \rangle. \tag{36}$$

---

[5]To obtain the energy bound (37) by a straightforward calculation, we have kept the $\nabla \cdot \mathbf{u}$ terms throughout the computation even though they are in fact zero.

Here the first line follows directly from integration by parts, noting that the boundary integrals vanish. The last equation can be written in a more compact form:

$$\frac{1}{2}\frac{\partial}{\partial t}\Big(||\nabla \times \mathbf{u}||^2 + ||\nabla \cdot \mathbf{u}||^2\Big) \;=\; -\mu||\mathcal{P}\Delta\mathbf{u}||^2. \tag{37}$$

From this it follows that the curl and divergence are bounded in the L^2 sense. As a first example of a semi-implicit scheme, we analyze the backward Euler discretization for the Stokes equation:

$$\left.\begin{aligned}
\mathbf{u}^{n+1} - \mathbf{u}^n - \Delta t\,\mu\,\Delta\mathbf{u}^{n+1} &= -\Delta t\,\nabla p^n & \text{for } \mathbf{x} &\in \Omega, \\
\mathbf{n} \times \mathbf{u}^{n+1} &= 0 & \text{for } \mathbf{x} &\in \partial\Omega, \\
\nabla \cdot \mathbf{u}^{n+1} &= 0 & \text{for } \mathbf{x} &\in \partial\Omega,
\end{aligned}\right\} \tag{38}$$

and

$$\left.\begin{aligned}
\Delta p^n &= 0 & \text{for } \mathbf{x} &\in \Omega, \\
\mathbf{n} \cdot \nabla p^n &= \mathbf{n} \cdot \mu\,\Delta\mathbf{u}^n & \text{for } \mathbf{x} &\in \partial\Omega.
\end{aligned}\right\} \tag{39}$$

We note that the scheme (38)–(39) preserves the divergence free condition on the velocity exactly. Assume $\nabla \cdot \mathbf{u}^n = 0$ for $\mathbf{x} \in \Omega$. Taking the divergence of (38), and setting $\phi(\mathbf{x}) = \nabla \cdot \mathbf{u}^{n+1}$ yields

$$\left.\begin{aligned}
-\Delta t\,\mu\,\Delta\phi &= -\phi & \text{for } \mathbf{x} &\in \Omega, \\
\phi &= 0 & \text{for } \mathbf{x} &\in \partial\Omega,
\end{aligned}\right\} \tag{40}$$

Since $-\Delta$ does not have a negative eigenvalue, $\phi = 0$ for all $\mathbf{x} \in \Omega$ is the only solution to (40). Consequently, the pressure equation for p^{n+1} automatically satisfies the Neumann consistency condition and is therefore well defined. As a direct consequence of preserving the divergence condition, the pressure as defined by (39) is equivalent to the projection:

$$\nabla p^n = \mathcal{Q}\Delta\mathbf{u}^n. \tag{41}$$

Remark 9. Since the scheme (38)–(39) preserves the divergence constraint, there is never the need for a projection step (ie. one may associate $\mathbf{u}^{n+1} = \mathbf{u}^{*n+1}$, where $\mathbf{u}^{*n+1}$ is the conventional intermediate velocity field with non-zero divergence). ♣

A stability proof for equations (38)–(39) closely follows the one for periodic channel flow in [24]. Specifically, dot both sides of equation (38) by $-\Delta(\mathbf{u}^{n+1} + \mathbf{u}^n)$, and integrate (this is the discrete analog of the steps required to derive equation (37)). The first two terms on the left hand side of equation (38) become

$$
\begin{aligned}
\langle \mathbf{u}^{n+1} - \mathbf{u}^n, -\Delta(\mathbf{u}^{n+1} + \mathbf{u}^n) \rangle \quad = \quad & ||\nabla \times \mathbf{u}^{n+1}||^2 + ||\nabla \cdot \mathbf{u}^{n+1}||^2 \quad (42) \\
& - \quad ||\nabla \times \mathbf{u}^n||^2 - ||\nabla \cdot \mathbf{u}^n||^2. \quad (43)
\end{aligned}
$$

In addition, we have

$$
\langle \Delta \mathbf{u}^{n+1}, \Delta(\mathbf{u}^{n+1} + \mathbf{u}^n) \rangle = \frac{1}{2}||\Delta \mathbf{u}^{n+1} + \Delta \mathbf{u}^n||^2 + \frac{1}{2}||\Delta \mathbf{u}^{n+1}||^2 - \frac{1}{2}||\Delta \mathbf{u}^n||^2, (44)
$$

and

$$
\langle \mathcal{Q}\Delta \mathbf{u}^n, \Delta(\mathbf{u}^{n+1} + \mathbf{u}^n) \rangle = \frac{1}{2}||\mathcal{Q}\Delta \mathbf{u}^{n+1} + \mathcal{Q}\Delta \mathbf{u}^n||^2 + \frac{1}{2}||\mathcal{Q}\Delta \mathbf{u}^n||^2 - \frac{1}{2}||\mathcal{Q}\Delta \mathbf{u}^{n+1}||^2. (45)
$$

For brevity, we also introduce the energy $\mathcal{E}$ where

$$
\mathcal{E}[\mathbf{u}] = ||\nabla \times \mathbf{u}||^2 + ||\nabla \cdot \mathbf{u}||^2 + \mu\Delta t||\Delta \mathbf{u}||^2 + \mu\Delta t||\mathcal{Q}\Delta \mathbf{u}||^2. \quad (46)
$$

Finally, combining everything, we have

$$
\begin{aligned}
\mathcal{E}[\mathbf{u}^{n+1}] - \mathcal{E}[\mathbf{u}^n] \quad = \quad & -\frac{\mu\Delta t}{2}||\Delta \mathbf{u}^{n+1} + \Delta \mathbf{u}^n||^2 + \frac{\mu\Delta t}{2}||\mathcal{Q}\Delta \mathbf{u}^{n+1} + \mathcal{Q}\Delta \mathbf{u}^n||^2 \quad (47) \\
= \quad & -\frac{\mu\Delta t}{2}||\mathcal{P}\Delta \mathbf{u}^{n+1} + \mathcal{P}\Delta \mathbf{u}^n||^2, \quad (48)
\end{aligned}
$$

so that

$$
\mathcal{E}[\mathbf{u}^{n+1}] \leq \mathcal{E}[\mathbf{u}^n]. \quad (49)
$$

For simply connected domains, the energy bound (49) implies the scheme (38)–(39) is unconditionally stable. Unfortunately the bound (49) is not sufficient to prove stability in periodic domains, or domains with holes. The reason here is that $\mathcal{E}[\mathbf{h}] = 0$ for any vector field $\mathbf{h}$ that has $\nabla \cdot \mathbf{h} = \nabla \times \mathbf{h} = 0$ in Ω, and $\nabla \cdot \mathbf{h} = \mathbf{n} \times \mathbf{h} = 0$ in $\partial\Omega$. In simply connected domains, the only such vector fields are $\mathbf{h} = 0$. On the other hand, in periodic domains or domains with holes, there exist vector fields $\mathbf{h} \neq 0$, which satisfy $\nabla \cdot \mathbf{h} = 0$ and $\mathbf{n} \times \mathbf{h} = 0$ on $\partial\Omega$ and $\mathcal{E}[\mathbf{h}] = 0$. Here the energy bound (49) does not control the growth of these modes. We note however that such vector fields $\mathbf{h}$ have non zero flux $\mathbf{h} \cdot \mathbf{n} \neq 0$ at the boundary. Hence, we expect that the modified scheme (20)–(20) with addition of the term $\lambda \mathbf{n} \cdot \mathbf{u}$ in the boundary condition for the pressure will stabilize the growth of such modes.

5.1. Stability of a second order scheme

Following a procedure analogous to the one in [24], we discuss the stability of a second order Crank-Nicholson scheme where we treat the pressure with a second order Adams-Bashforth extrapolation:

$$\left.\begin{aligned}
\mathbf{u}^{n+1} - \mathbf{u}^n &= \tfrac{\mu}{2}\Delta t\left(\Delta\mathbf{u}^{n+1} + \Delta\mathbf{u}^n\right) - \tfrac{3}{2}\Delta t\nabla p^n + \tfrac{1}{2}\Delta t\nabla p^{n-1} && \text{for } \mathbf{x} \in \Omega, \\
\mathbf{n} \times \mathbf{u}^{n+1} &= 0 && \text{for } \mathbf{x} \in \partial\Omega, \\
\nabla \cdot \mathbf{u}^{n+1} &= 0 && \text{for } \mathbf{x} \in \partial\Omega,
\end{aligned}\right\} \tag{50}$$

where p^n is given by (39). Proceeding with a normal mode analysis[6], we set $\mathbf{u}^n = \alpha^n\tilde{\mathbf{u}}$ where $\tilde{\mathbf{u}}$ satisfies the boundary conditions in (50), and α is an eigenvalue of the time stepping operator. Upon substitution we obtain

$$(\alpha^2 - \alpha)\tilde{\mathbf{u}} = \frac{\mu}{2}\Delta t(\alpha^2 + \alpha)\Delta\tilde{\mathbf{u}} - \frac{3}{2}\Delta t\alpha\mathcal{Q}\Delta\tilde{\mathbf{u}} + \frac{1}{2}\Delta t\mathcal{Q}\Delta\tilde{\mathbf{u}}. \tag{51}$$

In analogy with the steps in the previous section, we dot equation (51) through by $-\Delta\tilde{\mathbf{u}}$ and integrate by parts to obtain

$$2(\alpha^2 - \alpha)\left(||\nabla \times \tilde{\mathbf{u}}||^2 + ||\nabla \cdot \tilde{\mathbf{u}}||^2\right) + \mu\Delta t(\alpha^2 + \alpha)||\Delta\tilde{\mathbf{u}}||^2 = \mu\Delta t(3\alpha - 1)||\mathcal{Q}\Delta\tilde{\mathbf{u}}||^2. \tag{52}$$

Equation (52) is now a quadratic of the form $a\alpha^2 - b\alpha + c = 0$ for the eigenvalues α where

$$
\begin{aligned}
a &= 2||\nabla \times \tilde{\mathbf{u}}||^2 + 2||\nabla \cdot \tilde{\mathbf{u}}||^2 + \mu\Delta t||\Delta\tilde{\mathbf{u}}||^2, & (53) \\
b &= 2||\nabla \times \tilde{\mathbf{u}}||^2 + 2||\nabla \cdot \tilde{\mathbf{u}}||^2 - \mu\Delta t||\Delta\tilde{\mathbf{u}}||^2 + 3\mu\Delta t||\mathcal{Q}\Delta\tilde{\mathbf{u}}||^2, & (54) \\
c &= \mu\Delta t||\mathcal{Q}\Delta\tilde{\mathbf{u}}||^2. & (55)
\end{aligned}
$$

Since the coefficients a, b, c satisfy the following inequalities $0 \le c < a$ and $|b| < a+c$, it follows [46] that the eigenvalues α lie within the unit circle. The preceding argument indicates that the normal modes $\tilde{\mathbf{u}}$ remain bounded for the second order Crank-Nicholson scheme (50). Hence the scheme is stable for domains with simple geometries[7].

---

[6]We will not discuss here the question of whether the resulting eigenvectors form a complete basis.

[7]Note that in domains which are not simply connected, and have nontrivial homology groups, there is a family of harmonic modes which satisfy $\Delta\tilde{\mathbf{u}} = 0$. For these modes one can check that $a = b = c = 0$ and the argument fails to show that $|\alpha| < 1$

6. A First-Order Explicit Scheme on Irregular Domains

In this section we outline an explicit numerical scheme for solving the coupled differential equations (20–21) on a two-dimensional irregular domain. To achieve such a scheme, we decouple the pressure and velocity fields, and explicitly treat each term in the time evolution of (20–21). Specifically, since both the right hand side and boundary conditions of equation (21) depend solely on $\mathbf{u}$, we may view the pressure as a computable functional of the velocity, $p = p[\mathbf{u}]$. The computation of $p[\mathbf{u}]$ requires the solution of a Poisson equation with Neumann boundary conditions. With this in mind, the momentum equation then has the form $\mathbf{u}_t = \mathbf{F}[\mathbf{u}]$, where $\mathbf{F}[\mathbf{u}]$ has a complicated, yet numerically computable form:

$$\mathbf{F}[\mathbf{u}] = \mu \, \Delta \mathbf{u} - \nabla p[\mathbf{u}] - (\mathbf{u} \cdot \nabla) \, \mathbf{u} + \mathbf{f} \quad \text{for} \ \ \mathbf{x} \in \Omega. \tag{56}$$

We now use an explicit forward Euler scheme to discretize the time evolution for (20–21), paired with an appropriate discretization in space described later in this section. This yields the scheme

$$\frac{1}{\Delta t} \left(\mathbf{u}^{n+1} - \mathbf{u}^n \right) = \mu \, \Delta \mathbf{u}^n - \nabla p^n - (\mathbf{u}^n \cdot \nabla) \, \mathbf{u}^n + \mathbf{f}^n \quad \text{for} \ \ \mathbf{x} \in \Omega, \tag{57}$$

with boundary conditions $\mathbf{n} \times \mathbf{u} = \mathbf{n} \times \mathbf{g}$ and $\nabla \cdot \mathbf{u} = 0$ for $\mathbf{x} \in \partial\Omega$, where the pressure is given by

$$\Delta p^n = -\nabla \cdot \left((\mathbf{u}^n \cdot \nabla) \, \mathbf{u}^n \right) + \nabla \cdot \mathbf{f}^n \quad \text{for} \ \ \mathbf{x} \in \Omega, \tag{58}$$

with the boundary condition

$$\mathbf{n} \cdot \nabla p^n = \mathbf{n} \cdot \left(\mathbf{f}^n - \mathbf{g}_t^n + \mu \, \Delta \mathbf{u}^n - (\mathbf{u}^n \cdot \nabla) \, \mathbf{u}^n \right) + \lambda \, \mathbf{n} \cdot \left(\mathbf{u}^n - \mathbf{g}^n \right)$$

for $\mathbf{x} \in \partial\Omega$. Here, starting with the initial data $\mathbf{u}^0$, a superscript n is used to denote a variable at time $t = n \, \Delta t$, where $0 < \Delta t \ll 1$ is the time step.

Remark 10. Our purpose here is to illustrate the new approach with a simple scheme that does not obscure the ideas in the method with technical complications. Hence, the scheme here is first order in time (explicit) and second order in space, with the stability restriction $\Delta t \propto (\Delta x)^2$. However, unlike projection methods and other approaches commonly used to solve the Navier-Stokes equations — see § 1, this new formulation does not seem to have any inherent order limitations. Unfortunately, the Navier-Stokes equations are stiff and nonlinear, which means that the fact that higher order extensions are possible does not mean that they are trivial. ♣

6.1. Space grid and discretization.

To discretize the equations in space, we use finite differences over a carte-sian, square ($\Delta x = \Delta y$), staggered grid. The pressure values are stored at the nodes of the grid, while the horizontal and vertical components of the velocity are stored at the mid-points of the edges connecting the grid nodes (horizontal component on the horizontal edges and vertical component on the vertical edges).

When handling an arbitrary curved boundary, we do not conform the boundary to the grid, but rather we immerse it within the regular mesh — see figure 1. Then, to numerically describe the domain boundary, we identify a set $\mathcal{C}_b$ of N_e points in $\partial\Omega$, say $\mathbf{x}_{bj} = (x_b,\, y_b)_j$ for $1 \le j \le N_e$ — see item 6c below. These N_e points are located at $O(\Delta x)$ distances apart, so that the resolution of the boundary is comparable with that of the numerical grid.
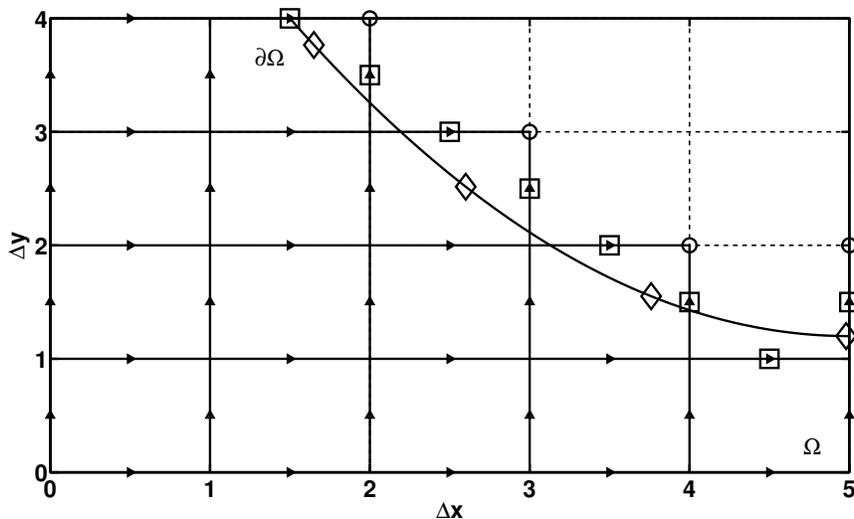
Figure 1: This plot shows the staggered grid, and the boundary. The numer-ical pressure values correspond to the graph nodes, while the velocities (ar-rows) correspond to the edge midpoints. Here the circles ($\circ$) and squares ($\square$) denote ghost pressure points, and boundary velocities, respectively. These are used to implement the boundary conditions in the Poisson and momen-tum equations, respectively. The diamonds ($\lozenge$) denote the points $(x_b,\, y_b)_i$, used to represent the boundary $\partial\Omega$.

For the heat equation $T_t = \mu\,\Delta T$, the stability restriction for the standard

scheme using a 5 point centered differences approximation for the Laplacian, and forward Euler in time, is

$$\Delta t \leq C \, \frac{(\Delta x)^2}{\mu}, \tag{59}$$

where $C = \frac{1}{2D}$ and $D = 1, 2, \ldots$ is the space dimension. Since the method described here uses exactly the same approach to advance the velocity flow field $\mathbf{u}$, we expect the same restriction (with, perhaps, a different constant C) to apply. For the 2D numerical calculations presented in § 7, we found that the algorithm was stable with $C \leq 0.2$, while $C \geq 0.3$ generally produced unstable behavior. Below we separately address the numerical implementation of equations (57) and (58).

6.2. Poisson Equation

To solve the pressure Poisson equation (58) with Neumann boundary conditions, we use the ghost point idea with a method by Greenspan [14] to implement the boundary conditions. As discussed above, we embed the domain Ω within a cartesian square grid, and classify the computational points in the grid into inner and ghost points (see next paragraph). Then: (i) for the inner points we discretize the Laplace operator using the standard 5 point centered differences stencil. (ii) For the ghost points we obtain equations from an appropriate discretization of the Neumann boundary condition. In particular, if there are N_a inner points, and N_b ghost points, then the discretized pressure is represented by a vector $\widehat{p} \in \mathbb{R}^N$ where $N = N_a + N_b$.

The computational domain, $\mathcal{C}_p$, for the pressure is comprised by the *inner* points and the *ghost* points, defined as follows:

6a The *inner* points are the points in the cartesian grid located inside Ω.

6b The *ghost* points are the points in the cartesian grid that are either outside Ω or on $\partial \Omega$, and which are needed to complete the 5 point stencil for some inner point.

6c Construct the set $\mathcal{C}_b$ used to track the boundary $\partial \Omega$ as follows: For every pressure ghost point in the grid: $\mathbf{x}_j^{pg}$, $1 \leq j \leq N_b$, select the closest point in the boundary $\mathbf{x}_{bj} \in \partial \Omega$. We will use these points to produce equations that approximate the Neumann boundary conditions (one equation per point). Thus, with this choice for $\mathcal{C}_b$, $N_e = N_b$.

It follows that, on the computational domain $\mathcal{C}_p$, the Poisson equation (including the boundary conditions) is discretized by N_a equations inside Ω, and N_b equations derived from the boundary conditions. Specifically

6d We use the standard 5 point centered differences stencil for the Laplacian, to obtain one equation for each of the N_a inner points. Similarly, we use a second order approximation for the forcing terms on the right hand side of the equation.

6e We construct one boundary condition equation for each pressure ghost point $\mathbf{x}_j^{pg}$, $1 \leq j \leq N_b$. This is done by building an extrapolation operator which acts on 6 nearby points from the computational domain to obtain a second order approximation to the normal derivative at the corresponding point $\mathbf{x}_{bj} \in \partial\Omega$ — see item 6c above. The 6 points are comprised of the 5 point stencil used to approximate the Laplacian, plus one of the four next closest points to the center point. The extrapolation operator, which contains 6 coefficients, is then build to linearly interpolate the normal derivative using local values of the pressure. Hence each boundary point provides one equation coupling six values of the pressure.

We use a similar extrapolation operator to approximate the terms on the right hand side of the Neumann boundary conditions.

Hence, each boundary condition equation involves the ghost point, points inside the domain, and (possibly) other nearby ghost points.

Thus the Poisson equation can be written in a matrix form with the following structure

$$
\begin{pmatrix} L \\ B \end{pmatrix} \widehat{p} = \begin{pmatrix} a \\ b \end{pmatrix}. \tag{60}
$$

Here $B \in \mathbb{R}^{N_b \times N}$ and $L \in \mathbb{R}^{N_a \times N}$ are the discrete matrix representations for the derivatives $(\mathbf{n} \cdot \nabla)$ in the Neumann boundary condition, and Laplacian (Δ), respectively. The terms $a \in \mathbb{R}^{N_a}$ and $b \in \mathbb{R}^{N_b}$ are the discrete representations of the source terms and applied boundary conditions for the Poisson equation:

$$
\begin{aligned}
a &\approx \nabla \cdot (\mathbf{f} - (\mathbf{u} \cdot \nabla)\,\mathbf{u})\,, \tag{61} \\
b &\approx \mathbf{n} \cdot (\mathbf{f} - \mathbf{g}_t + \mu\,\Delta\,\mathbf{u} - (\mathbf{u} \cdot \nabla)\,\mathbf{u}) + \\
&\quad \lambda\,\mathbf{n} \cdot (\mathbf{u} - \mathbf{g}). \tag{62}
\end{aligned}
$$

24

Thus the pair of equations

$$L\widehat{p} = a \quad \text{and} \quad B\widehat{p} = b \tag{63}$$

are the discrete analog of equation (21).

Remark 11. For domains where the velocity is specified on the boundary, the pressure is only determined up to a constant. Hence, the discrete linear system (60) is singular, and discretization errors in a and b may cause solvability for equation (60) to fail. These solvability errors arise from numerical truncation, and are therefore "small" (second order). Hence, as it is commonly the case with numerical solutions of the Poisson equation with Neumann boundary conditions, we project the right hand side of (60) onto the column space of the Poisson matrix. For a conscise approach, on how to solve the system by constructing a square, nonsingular matrix system using the null vector $r = [11 \ldots 1]^T$, see [19]. ♣

6.3. Momentum Equation

The main numerical difficulty with implementing (57) is produced by the boundary conditions. Specifically: on a cartesian staggered grid the boundary conditions $\nabla \cdot \mathbf{u} = 0$ and $\mathbf{n} \times (\mathbf{u} - \mathbf{g}) = 0$ couple the "horizontal", u, and "vertical", v, components of the flow velocity — with the exception of the special case of a boundary aligned with the grid, where there is no coupling. Hence, in general, the implementation of the boundary conditions requires the solution (at every time step) of a linear system of equations that couples all the boundary velocities (these are defined below). It may be possible to avoid the difficulties with the boundary conditions discussed in this section by using a different spatial discretization. For example, overlapping grids which conform to the domain boundaries, such as those found in [19, 21], may avoid the coupling between velocity boundary components.

The *computational domain for the velocities*, $\mathcal{C}_\mathbf{u}$, is defined in terms of the edges in the cartesian grid with which the velocities are associated (see figure 1). To define $\mathcal{C}_\mathbf{u}$, it is convenient to first introduce the *extended set of pressure nodes*, $\mathcal{E}_p$, from which $\mathcal{C}_\mathbf{u}$ is easily constructed:

6f A pressure node in the cartesian grid belongs to $\mathcal{E}_p$ if and only if it either belongs to $\mathcal{C}_p$, or if it is connected (by an edge in the grid) to a ghost pressure node that lies on $\partial\Omega$.

6g A velocity is in $\mathcal{C}_\mathbf{u}$ if and only if: (a) Its corresponding edge connects two points in $\mathcal{E}_p$. (b) At least one of the two points is in Ω (or $\partial\Omega$).

Remark 12. Notice that $\mathcal{E}_p$ is exactly what $\mathcal{C}_p$ becomes if $\partial\Omega$ is modified by an "infinitesimal" perturbation that turns all the ghost pressure points on $\partial\Omega$ into inner pressure points.

The computational domain $\mathcal{C}_\mathbf{u}$ is, in turn, sub-divided into inner and boundary velocity edges

6h An edge in $\mathcal{C}_\mathbf{u}$ is an *inner* velocity if and only if $\mathcal{C}_\mathbf{u}$ includes the four other edges needed to compute the Laplacian (either Δu or Δv) at the edge mid-point, using the 5 point centered differences approximation.

6i An edge in $\mathcal{C}_\mathbf{u}$ is a *boundary* velocity if and only if it is not an inner velocity. Let M *be the number of boundary velocities.*

The solution of the momentum equation (20) is thus performed as follows:

6j At the start of each time step the right hand side in (57) is approximated (to second order, using centered differences) at the inner velocity locations, which can then be updated to their values at the next time.

6k Next, using the boundary conditions, the values of the boundary velocities at the next time step are constructed from the inner velocities. This "extension" process is explained below.

Let $\mathbf{y} \in \mathbb{R}^M$ be the vector of boundary velocities. Then $\mathbf{y}$ is determined by two sets of equations, corresponding to the discretization on $\partial\Omega$ of $\nabla \cdot \mathbf{u} = 0$ and $\mathbf{n} \times (\mathbf{u} - \mathbf{g}) = 0$. In our approach the divergence free criteria is enforced "point-wise", while the condition on the tangential velocity is imposed in a least squares sense.

Implementation of the divergence free $\nabla \cdot \mathbf{u} = 0$ *boundary condition.* At first sight, this boundary condition appears to be the hardest to implement, since it is a Neumann condition (essentially) prescribing the value of the normal derivative of the normal component of the velocity, in terms of the tangential derivative of the tangential velocity. However, because (for the exact solution) $\nabla \cdot \mathbf{u} = 0$ everywhere, an implementation of this condition which is second order consistent (in the classical sense of finite differences introduced by Lax [30]) is easy to obtain, as follows:

26

First: identify the M_d pressure nodes in $\mathcal{C}_p$, which have at least one boundary velocity as an adjacent edge. These M_d pressure nodes lie either on $\partial\Omega$, or inside Ω, and are all within a distance $O(\Delta x)$ of $\partial\Omega$ — definitely no further away than $\sqrt{2}\,\Delta x$. Second: for each of these M_d points, use centered differences to approximate the flow divergence at the point, and set $\nabla\cdot\mathbf{u} = 0$. This provides M_d equations that couple the (unknown) boundary velocities to the (known) inner velocities. In matrix form this can be written as

$$D\mathbf{y} = \mathbf{s} \tag{64}$$

where D is the portion of the discrete divergence operator acting on the unknown boundary velocities, while $\mathbf{s}$ is the associated flux derived from the known inner velocities. D is a rectangular, very sparse, matrix whose entries are 0 and ± 1 — note that Δx can be eliminated from these equations.

Remark 13. Notice that $\nabla \cdot \mathbf{u} \equiv 0$ for the exact solution. Hence, setting $\nabla \cdot \mathbf{u} = 0$ at the nodes near the boundary (as done above) involves no approximation. The second order nature of (64) is caused by the error in computing $\nabla \cdot \mathbf{u}$ — there is no "extrapolation" error. ♣

Implementation of the tangential velocity $\mathbf{n} \times (\mathbf{u} - \mathbf{g}) = 0$ *boundary condition.* It is easy to see that $M_d \approx M/2$, since most of the M_d pressure nodes in the selected set will connect with two boundary boundary velocities. Thus (64) above provides approximately one half the number of equations needed to recover $\mathbf{y}$ from the inner velocities. It would thus seem natural to seek for $M - M_d$ additional equations using the other boundary condition. Namely, find $M - M_d$ points on $\partial\Omega$, and at each one of them write an approximation to $\mathbf{n} \times (\mathbf{u} - \mathbf{g}) = 0$ using nearby points in $\mathcal{C}_\mathbf{u}$. Unfortunately, this does not work. It is very hard to do the needed approximations in a fashion that is robust relative to the way Ω is embedded in the rectangular grid. Our attempts at this simple approach almost always lead to situations where somewhere along $\partial\Omega$ an instability was triggered.

To avoid the problem stated in the previous paragraph, we over-determine the implementation of the tangential velocity boundary condition, and solve the resulting system in the least squares sense. The boundary condition is replaced by the minimization of a (discrete version) of a functional of the form

$$\int_{\partial\Omega} |\mathbf{n} \times (\mathbf{u} - \mathbf{g})|^2 \, w \, \mathrm{d}A, \tag{65}$$

where w is some (strictly positive) weight function. This approach yields a robust, numerically stable, approximation — fairly insensitive to the particular details of how Ω is embedded within the cartesian grid.
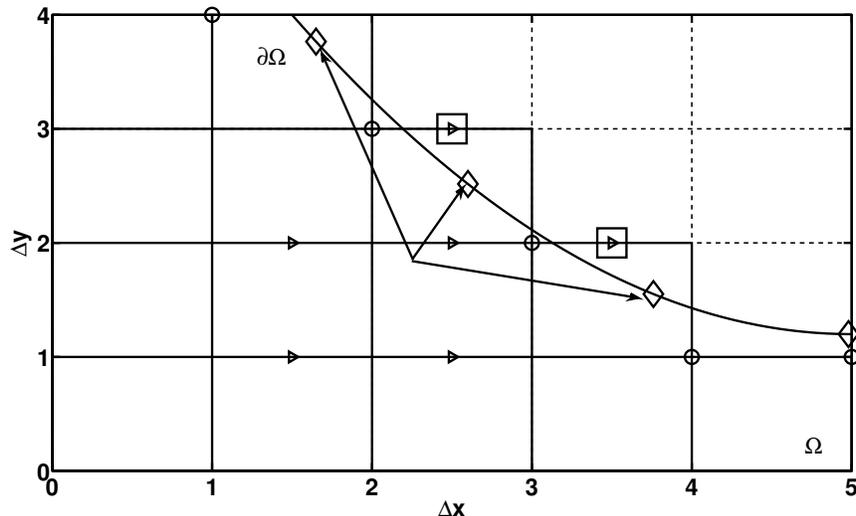

Figure 2: This plot illustrates the implementation of the momentum equation boundary conditions. The circles ($\circ$) indicate the points at which the velocity divergence is set to zero. The six arrows indicate the horizontal velocity components in the patch, $\mathcal{P}^u_{j\nu}$, used to extrapolate u to the three boundary points indicated by the diamonds ($\Diamond$). The squares ($\Box$) denote the boundary velocities — which are part of the patch $\mathcal{P}^u_{j\nu}$.

In fact, we do not implement the minimization of a functional as in (65), but a simpler process which is (essentially) equivalent. To be specific, we start with the set $\mathcal{C}_b$ of points in $\partial\Omega$ — see item 6c. For each $\mathbf{x}_{bj} \in \mathcal{C}_b$, where $1 \leq j \leq N_e$, we identify a local horizontal, $\mathcal{P}^u_j$, and vertical, $\mathcal{P}^v_j$, velocity "patch". These patches — see figure 2 — have the following properties

6l Each patch contains both inner and boundary velocities.

6m Each patch contains 6 velocities, in an appropriate structure, so that these velocities can be used to extrapolate (with second order accuracy) values of the corresponding velocity (u or v) to nearby points along the boundary. For example: the 5 point stencil used to approximate the Laplacian, plus one of the four next closest points to the center point.

6n The union of all the patches contains all the boundary velocities.

These patches are used to (linearly) interpolate/extrapolate the velocities to nearby points along the boundary. For example, the horizontal velocity at point $\mathbf{x}_{bj}$ is extrapolated using patch $\mathcal{P}_j^u$ by

$$u|_{\mathbf{x}_{bj}} = \sum_{\mathbf{x}_k \in \mathcal{P}_j^u} \gamma_k u_k \tag{66}$$

where u_k is the velocity at $\mathbf{x}_k$, and γ_k are precomputed coefficients which linearly extrapolate u to second order.

Each patch is used to extrapolate the velocity to the three "closest" boundary points to the patch. In this fashion, for every $\mathbf{x}_{bj}$, $1 \le j \le N_e$, three different approximations to the tangential velocity at the boundary follow. These involve different (linear) combinations of velocities at the nearby edges in $\mathcal{C}_\mathbf{u}$, including both boundary and inner velocities. In this fashion, a set of $3\,N_e$ additional linear equations — beyond those in equation (64) — for the boundary velocities follow.

Remark 14. The idea in the process above is to "link" the patches used to extrapolate the velocity to the boundary. This is so that no "gaps" occur in the implementation of the tangential boundary conditions, as the positioning of $\partial\Omega$ relative to the grid changes. We elected to use minimal coupling (each patch linked to its two neighbors). In principle one could increase the amount of over-determination of the tangential boundary condition. This would require using a set of points in $\partial\Omega$ that is "denser" than $\mathcal{C}_b$, but *in our calculations we found that this was not needed.*

Finally, an interesting question is: why is a process similar to this one not needed for the implementation of the boundary conditions for the Poisson equation in § 6.2? The obvious answer is that the Poisson equation itself couples everything, so that no extra coupling needs to be added. ♣

Putting everything together, an overdetermined system of equations for the boundary velocity vector $\mathbf{y}$ follows, which can be written in the form

$$D\mathbf{y} = \mathbf{s}, \tag{67}$$
$$E\mathbf{y} = \mathbf{t}. \tag{68}$$

Here $E \in \mathbb{R}^{3\,N_e \times M}$, and the second equation is to be solved in the least squares sense, subject to the constraint imposed by the first equation. One

way to do this is as follows: write

$$\mathbf{y} = \mathbf{y}_p + P\mathbf{c} \tag{69}$$

where P is a matrix whose columns are a basis for the kernel of D — hence $DP = 0$, $\mathbf{y}_p$ is a particular solution of (67), and $\mathbf{c}$ is a constant vector parameterizing the space of (numerical) divergence free boundary velocities. Substituting the ansatz (69) into (68) yields

$$(E\,P)\,\mathbf{c} = \mathbf{t} - E\,\mathbf{y}_p, \tag{70}$$

which is a constraint-free least squares problem for the vector $\mathbf{c}$. Thus we can write

$$\mathbf{c} = (E\,P)^+\,(\mathbf{t} - E\mathbf{y}_p), \tag{71}$$

which, together with (69), gives the solution $\mathbf{y}$.

Remark 15. In (71), $(E\,P)^+$ is the pseudo-inverse, defined by the singular value decomposition of the matrix $F = E\,P$. In fact, since $F^T\,F$ should be invertible (see below), $F^+ = (F^T\,F)^{-1}\,F^T$.

One of the objectives of the above construction is to ensure that the boundary velocities are completely determined by the boundary conditions (and the inner velocities). If the problem in (68) for $\mathbf{y}$, with the constraint in (67), were to have more than one solution that minimizes the L^2 norm of $\mathbf{t} - E\,\mathbf{y}$, then this would be a sure sign that the boundary condition implementation is flawed, and there is missing information (i.e.: more equations are needed, see remark 14).

Of course, the requirement in the prior paragraph is equivalent to the statement that $F^T\,F$ is invertible. Finally, notice that in a domain with a fixed boundary, one may preprocess the matrices E, D and P. ♣

Remark 16. It should be clear that the scheme developed in this section, is second order consistent[8] (all the way up to the boundary) in the classical sense of finite differences introduced by Lax [30]. ♣

---

[8]For the system of PDE in (20–21).

6.4. Comparison with the Projection Method

The scheme proposed here — which involves the implementation of the equations in (57–58), appears to be quite similar to fractional step methods, such as Chorin's [7] original projection method. Specifically: advancing one time step requires both the evolution of a diffusion equation for the flow velocity, and the inversion of a Poisson equation for the pressure — which is the same as in projection methods. But there are important differences, mainly related to the implementation of the boundary conditions, and of the incompressibility condition. Below we highlight the similarities and differences between the pressure Poisson approach proposed here and, for simplicity, the projection method in its original formulation [7]. A (fairly recent) thorough review of projection methods, exploring the improvements to the approach since [7], as well as their drawbacks, can be found in [16].

First, the starting point for the method here is the discretization of a reformulation of the equations: (20–21), not the "original" Navier-Stokes equations (1–2). In this equivalent set: (i) there is a natural way to recover the pressure from the flow field at any given time. (ii) The time evolution automatically enforces incompressibility. As a consequence, there is (in-principle) no limitation to the order in time to which the reformulated equations can be numerically discretized. In contrast, the projection method is equivalent to an approximate LU matrix factorization [16, 36, 47] of the discrete differential operators coupling $\mathbf{u}$ and p. This approximate factorization yields a splitting error in time, which is very hard to circumvent in order to achieve higher accuracy.

Second, the pressure Poisson formulation used here ensures both that, at every point in the time integration: (i) the normal and tangential velocity boundary conditions are accurately satisfied. (ii) The zero divergence condition is accurately satisfied. On the other hand, in the original projection method, the step advancing the flow velocity forward in time enforces the velocity boundary conditions, but cannot guarantee that incompressibility is maintained. In the other step, the pressure is used to recover incompressibility — by projecting the flow velocity field onto the space of divergence free fields. Unfortunately, while removing the divergence, this second step does not necessarily preserve the correct velocity boundary values [16].

Finally the modified equation (57) implemented here differs from the projection's method velocity forward step primarily by the boundary conditions imposed. Specifically, the projection method imposes Dirichlet boundary conditions for each component of the velocity field when propagating the

flow velocity. Dirichlet boundary conditions have the obvious advantage of decoupling the velocity components. Numerically this means that an implicit treatment of the stiff viscosity operator $\partial_t - \mu\,\Delta$ is straightforward. By contrast, on a regular grid, the boundary conditions in (57) couple the boundary velocities. Although this coupling does not pose a serious difficulty for explicit schemes, it adds a (potentially serious) difficulty to the implementation of any scheme that treats the viscosity operator in the equations implicitly.

7. Implementation

The objective of this section is to study the convergence and accuracy of the schemes proposed in § 5 and § 6, and to test the methods for a simple physical problem. In particular: to verify the theoretical prediction that the temporal splitting in § 5 is second order in time, while the spatial discretization in § 6 is second order in space, all the way up to the boundary.

To this end, here we present the results from numerical computations for (i) Externally forced flow on a square domain in § 7.1, (ii) Computation of flow in a lid driven cavity in § 7.2, and (iii) Externally forced flow on an irregular domain in § 7.3. In examples (i) and (iii), the external forcing is selected so that an exact (analytic) solution to the equations can be produced, following the same procedure as in [16].[9] In what follows the numerical errors are measured using the discrete L^∞ grid norm defined by

$$\|g\|_\infty = \max\{|g_{ij}|\}. \tag{72}$$

Here the maximum is over all the indexes i and j — corresponding to the appropriate grid coordinates (x_i, y_j) in the computational domain — for the field g in the staggered grid. Namely: nodes for the pressure p, midpoints of the horizontal edges for u, and mid-points of the vertical edges for v. Note that neither ghost pressure points, nor boundary velocities, are included within the index set in (72) — we consider these as auxiliary numerical variables, introduced for the purpose of implementing the boundary conditions, but not part of the actual solution. Finally, for the exact (analytic) solution, grid values are obtained by evaluation at the points (x_i, y_j). For example, to compute the error in the pressure, first define the discrete

---

[9]That is, proceed backwards: first write an incompressible flow, and then compute the forcing, and boundary conditions, it corresponds to.

field $e_{ij} = \hat{p}_{ij} - p(x_i, y_j)$ — where $\hat{p}$ is the numerical pressure field and p is the exact continuous field, and then compute the norm above for e.

As should be clear from the prior sections, the main issue we aim to address in this paper, is that of how to effectively implement the incompressibility condition and the boundary conditions for the pressure, avoiding the difficulties that projection and fractional step methods have. These are problems that are not related to the nonlinearities in the Navier-Stokes equations, and occur even in the absence of the advective term $(\mathbf{u} \cdot \nabla)\mathbf{u}$. Hence, for simplicity, the calculations presented in subsections § 7.1 and § 7.3 do not contain the advective term. This is the same practice employed in [16]. Subsection § 7.2, however, investigates a physical flow and therefore includes the advective term.

7.1. Flow on a square domain

Here we test the semi-implicit scheme outlined in § 5. Specifically, we present the results of solving the linear Navier-Stokes equations on the unit square $0 \leq x, y \leq 1$, with no-slip and no flux boundary conditions (i.e.: $u = v = 0$ on $\partial \Omega$), and viscosity $\mu = 1$. We select the forcing function $\mathbf{f} = \mathbf{u}_t + \nabla p - \mu \Delta \mathbf{u}$ to yield the following (incompressible) velocity and pressure fields:

$$
\begin{align}
u(x, y, t) &= \pi \cos(t) \sin(2\pi y) \sin^2(\pi x), \tag{73}\\
v(x, y, t) &= -\pi \cos(t) \sin(2\pi x) \sin^2(\pi y), \tag{74}\\
p(x, y, t) &= -\cos(t) \cos(\pi x) \sin(\pi y). \tag{75}
\end{align}
$$

We numerically evolve the equations with varying grid and time steps. We then compare the numerical results with the exact fields in (73–75). For instance, figure 3 shows the error fields for the velocity and pressure at time $t = 4\pi$, for an 80×80 grid, time step $\Delta t = 0.2\,\Delta x$ and feedback $\lambda = 30$. Note that this test is essentially the same as the one used in [16][10], to test projection and fractional step methods. Hence the results in this subsection can be used as a comparison basis for the approach in this paper versus projection methods. Unlike the common situation with projection methods, in our case there are neither numerical boundary layers, nor numerical corner layers.
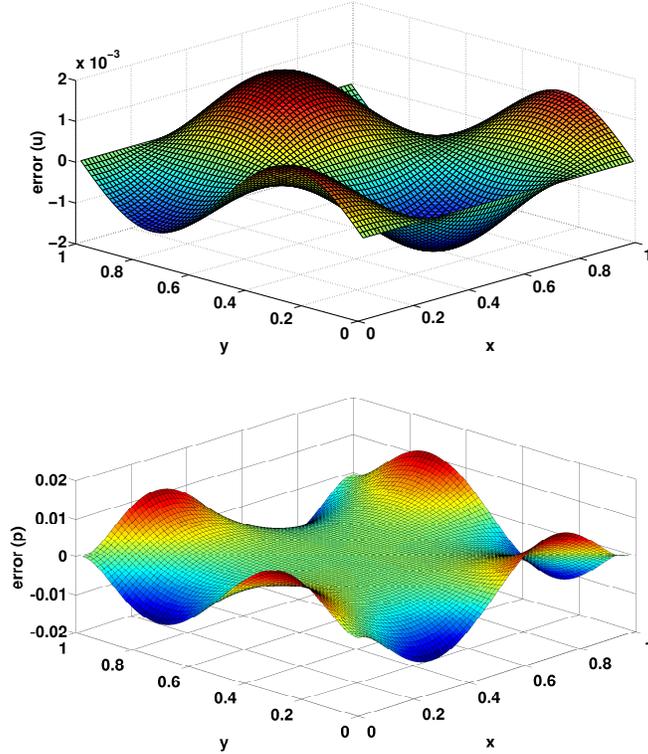
---

[10]See § 3.7.1, equation (3.30).

Figure 3: Error fields for the second order semi-implicit numerical scheme. The plots are at time $t = 4\pi$, for an 80×80 grid, with $\Delta t = 0.2 (\Delta x)$ and $\lambda = 100$. The horizontal velocity u (top) and the pressure p (bottom) error fields are shown. The error is uniform in size across the domain. There are neither numerical boundary layers, nor numerical corner layers.

To verify the scheme is second order in time, we fix a 220×220 grid and evolve the solution from $t = 0$ to $t = 1$ for varying Δt. Figure (4) shows second order convergence, while the saturation occurs when the spatial and temporal errors become comparable at $\Delta t \sim \Delta x$.

We now illustrate the role of the feedback parameter λ. For this purpose we present here the results of two tests. In the first test, we evolved the numerical solutions (with a fixed Δx) for different values of λ. [11] Figure 5

---

[11]With an 80×80 grid, viscosity $\mu = 1$ and a a time step $\Delta t = 0.2 (\Delta x)$.

34
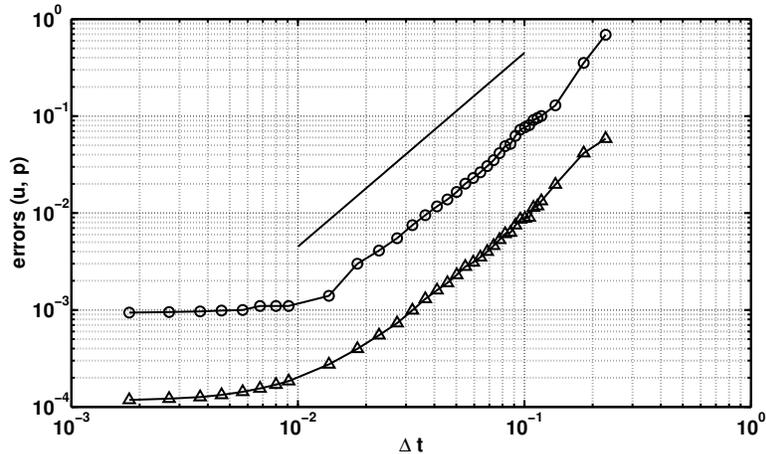
Figure 4: Convergence plot for semi-implicit numerical scheme. The plot corresponds to a fixed 220×220 grid and varying time steps ($\lambda = 30$). The straight line corresponds to second order convergence, while the saturation occurs around $\Delta t = \Delta x$ when the temporal errors become the same order as the spatial errors. The circles ($\circ$) and squares ($\square$) correspond to the L^∞ norm of the pressure and horizontal velocity respectively.

illustrates the results of this first test, with plots of the L^∞ error in the horizontal velocity u, as a function of time, for various values of λ. The errors in the pressure p, and in the vertical velocity v, exhibit the same qualitative behavior. In the absence of feedback — i.e. $\lambda = 0$, the errors grow steadily in time, as can be expected from equation (18) when influenced by the presence of numerical noise. Even though this effect does not constitute an instability (in the sense of exponential growth), there appears to be no bound to the growth. Thus, after a sufficiently long time, the errors can become substantial. The figure shows also that moderate values of λ — i.e. $\lambda \sim 10$ or bigger, are enough to control the errors.

Physically, the errors that occur when λ is too small correspond to fluid leakage through the domain walls. However, these errors cause little net mass loss or gain, since $\nabla \cdot \mathbf{u} = 0$ applies — actually, $\nabla \cdot \mathbf{u} = O\left((\Delta x)^2\right)$, as we show later: see figure 17. Any positive flow across some part of the boundary must be compensated by a negative flow elsewhere.

In the second test, we introduce artificial random errors to the normal velocity along the boundary. The purpose of this second test is to study, under
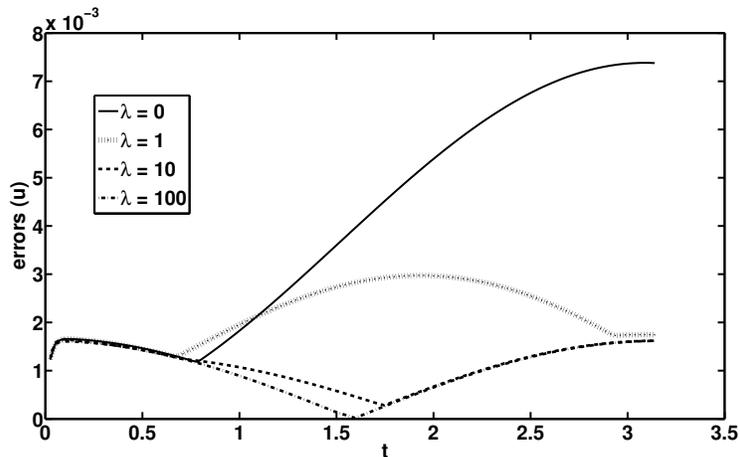
Figure 5: Time evolution of the L^∞ error in u on an 80×80 mesh. The flow is computed using the second order semi-implicit scheme with different values of the parameter λ. For $\lambda = 0$ the error grows in time. Values larger than $\lambda \sim 10$ control the error.

a controlled situation, the error sensitivity of the normal velocity boundary condition implementation — the purpose for which the parameter λ was introduced in § 4. Specifically, the main concern are the errors that are introduced by the implementation of the Neumann boundary condition for the pressure on non-conforming boundaries (as happens for the example in § 7.3).

To perform the test, we introduce independent random errors at each point on the domain boundary, at the start of each Euler time step. To be precise, the boundary condition for equation (58) is taken as

$$\mathbf{n} \cdot \nabla p^n = \mathbf{n} \cdot (\mathbf{f}^n + \Delta \mathbf{u}^n + \lambda \, \mathbf{u}^n) + r, \tag{76}$$

where, at each boundary point r is sampled randomly from the interval $[0, 1]$. This represents an $O(1)$ random perturbation to the normal component of the desired velocity, $\mathbf{g} = 0$, at the boundary.[12] Hence, it is a very demanding test of how insensitive the boundary condition implementation is to errors.

Figure 6 shows the error in the horizontal velocity u as a function of time, both for the feedback controlled solution with $\lambda = 100$, and the undamped

---

[12]Recall that in this section we take $\mu = 1$, and neglect the nonlinear terms.

36
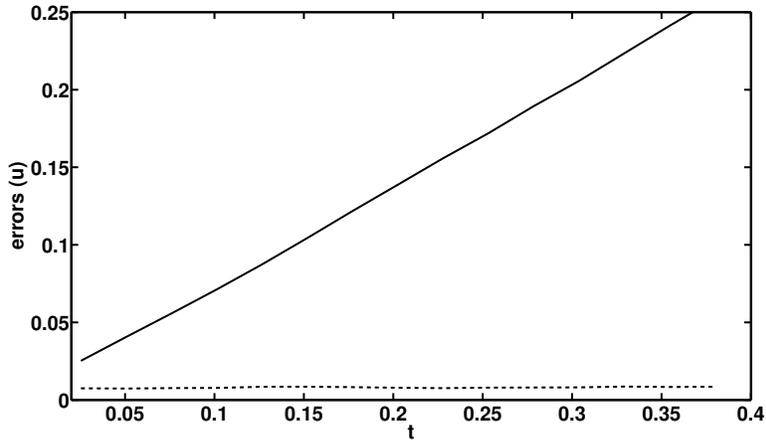
Figure 6: Time evolution of the L^∞ error in u on an 80×80 mesh. Flow is computed using a second order semi-implicit scheme and random forcing on the boundary. Without feedback ($\lambda = 0$, solid line) the error grows steadily. With feedback ($\lambda = 100$, dashed line) the error growth saturates at a small value.

solution with $\lambda = 0$. The errors saturate in the feedback solution, but they grow steadily for the undamped solution. Without damping, the drift errors contribute sizable effects to the solution after a short time period.

Finally, figure 7 illustrates the flow leakage produced by the random errors. This figure shows a cross section of the horizontal velocity u after time $t = 1$, for two values of the control parameter: $\lambda = 0$ and $\lambda = 100$. The first value shows a significant flow through the boundary, while the second does not. This plot also illustrates the point made earlier: there is no significant mass loss (gain) even when $\lambda = 0$, with positive flows compensated by negative flows elsewhere.

7.2. Driven Cavity

In this subsection, we solve for the fluid velocity field in a driven cavity. We use the second order semi-implicit scheme (50) and the regular staggered grid described in § 6. In addition, this test also demonstrates the application of a non-vanishing boundary condition where $\mathbf{n} \times \mathbf{u} \neq 0$. Here we include the nonlinear terms and treat them explicitly in the numerical scheme. To discretize them in space, we use a second order upwind (one sided) finite
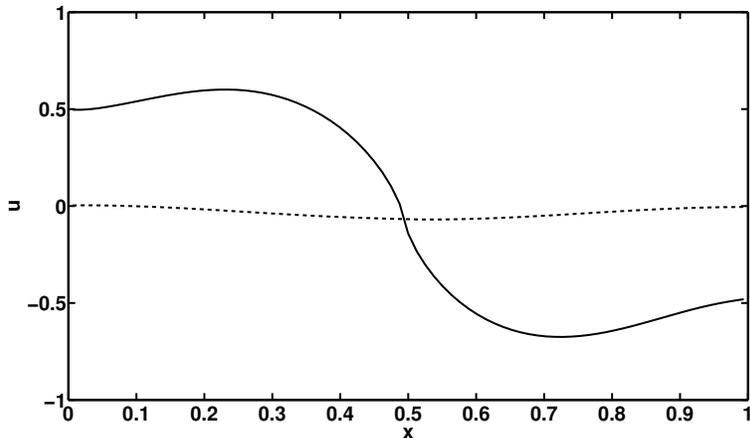
37

Figure 7: Velocity cross-section $u(x, y = 0.4937)$, at time $t = 1$, for the second order semi-implicit scheme, on an 80×80 mesh, with a random forcing on the boundary. The dashed line ($\lambda = 100$) reproduces the correct field with zero flux at the boundaries. The solid line ($\lambda = 0$) shows a non-zero flow through the boundary.

difference approximation. In this test, we take the velocity of the moving wall $U_{wall} = 1$ and consider different Reynolds numbers. Starting with rest initial conditions, we evolve the fields until they reach a steady state flow. Figures 8 and 9 show the midpoint steady state velocities for **u** at Reynolds numbers $Re = 100$ and $Re = 400$ respectively. The plots are done with a 220×220 grid and also compare the computation to the standard benchmark of [10]. In addition figure 10 shows the streamfunction contours for a Reynolds number of $Re = 400$.

7.3. Flow on an Irregular Domain

In this section we implement the numerical scheme described in § 6, for an example with an externally forced velocity field on an irregular shaped domain. We perform the same test, and take the same forcing from § 7.1 using equations (73–74) however, instead of the unit square, the selected domain Ω is the 1×1 square $0 < x, y < 1$, with the disk of radius $1/4$ centered at $(1/2, 1/2)$ removed. In addition, we use periodic boundary conditions in the y direction, and impose a nonzero flux ($\mathbf{u} = \mathbf{g} \neq 0$) on the rest of the boundary.
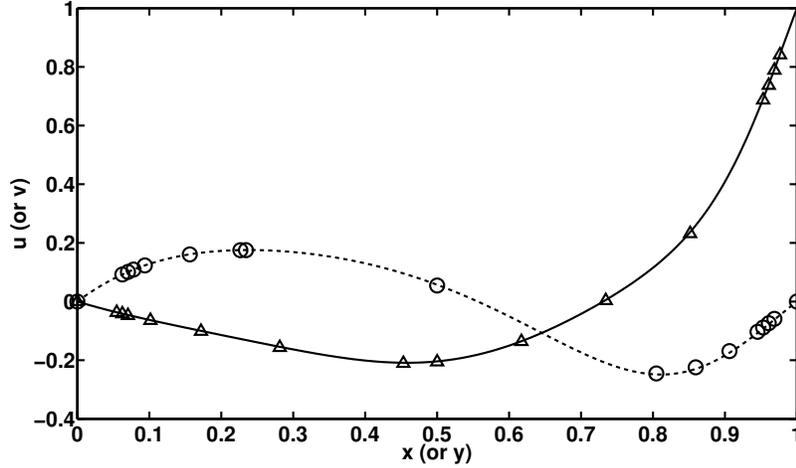
38

Figure 8: Midpoint steady state velocities (after $t = 20$) for $Re = 100$ and a 220×220 grid. For $\mathbf{u} = (u, v)$, the solid line shows $u(0.5, y)$, the dashed line shows $v(x, 0.5)$, while the circles and triangles correspond to data from [10].
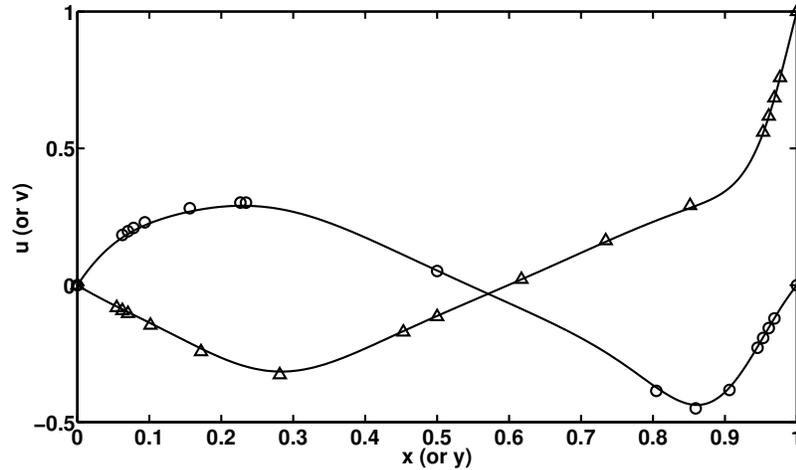

Figure 9: Midpoint steady state velocities (after $t = 30$) for $Re = 400$ and a 220×220 grid. For $\mathbf{u} = (u, v)$, the solid line shows $u(0.5, y)$, the dashed line shows $v(x, 0.5)$, while the circles and triangles correspond to data from [10].

In this example we set the feedback parameter λ to $\lambda = 100$, considerably larger than the minimum needed to get good behavior in the calculations in

39
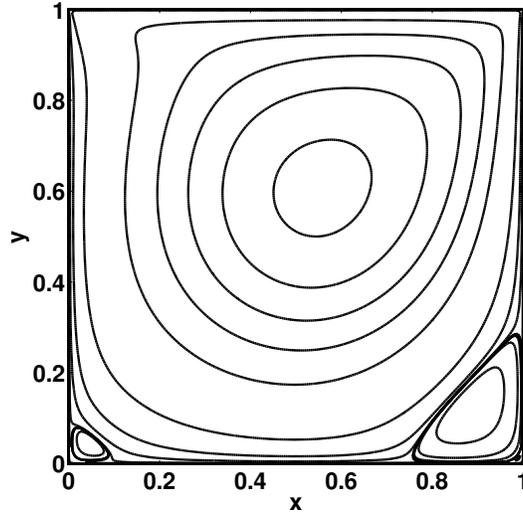
Figure 10: Plots shows steady state streamfunction contours for the driven cavity with $Re = 400$.

§ 7.1. This is to be expected from the results of the last test in § 7.1 — see figures 6 and 7. Because of the curved inner boundary in the current example, errors in the implementation of the Neumann boundary condition for the pressure occur, which trigger a drift in the normal boundary condition for the velocity — unless a large enough λ is used. Thus, for example, values where $\lambda = O(10)$ did not allow the feedback to quickly track fluctuations in the normal velocity component of the boundary conditions.

Second order convergence.

To illustrate the second order convergence of the scheme, below we present the results of evolving the velocity and pressure fields (for the problem described above), for varying grid sizes Δx, up to the fixed time $t = 0.0657$, using $\lambda = 100$ and $\Delta t = 0.2 \, (\Delta x)^2$. Note that the selected final time appears small, but it is large enough to require a number of time steps in the range $O(10^3)$ to $O(10^4)$ — for the grid sizes we used. This is large enough to provide a reliable measure of the order of the scheme.

Figure 11 shows the convergence of velocity and pressure, while figure 12 shows the convergence of the partial derivatives of the horizontal velocity
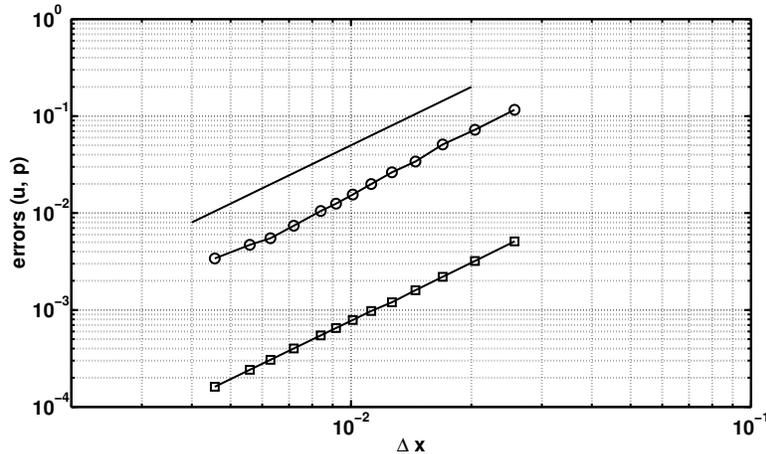
40

Figure 11: (Flow on an irregular domain example). Convergence plot for the pressure (circles: ○) and the horizontal velocity (squares: □). The errors (in the L^∞ norm) are computed at the fixed time $t = 0.0657$, for different grid resolutions, with $\Delta t = 0.2 \, (\Delta x)^2$. The slope of the solid straight line corresponds to the second order scaling error $\propto (\Delta x)^2$.

u. The figures indicate second order L^∞ convergence for the velocity u, the pressure p, and even the velocity gradient (u_x, u_y) — see § 7.4.

Typical error behavior.

We illustrate the (typical) error behavior — both in time and in space, by showing the results of a calculation done at a fixed resolution. Specifically, we take an 80×80 grid, with $\Delta t = 0.2(\Delta x)^2$ and $\lambda = 100$, and solve the forced system of equations in this "flow on an irregular domain" example — recall that $\mu = 1$.

Figure 13 shows the time evolution of the L^∞ (spatial) error in the horizontal velocity. It should be clear that, while the errors oscillate (over almost one decade in amplitude), they do not exhibit any measurable growth with time.

Figure 14 shows the horizontal velocity field at time $t = 4\pi$, while figure 15 shows the associated error field. Notice that, while the error is largest near the boundary — as expected from the difficulties that a curved, non-conforming, boundary causes — it is fairly well behaved, without abrupt transitions on the scale of the grid size. This explains why the error in the
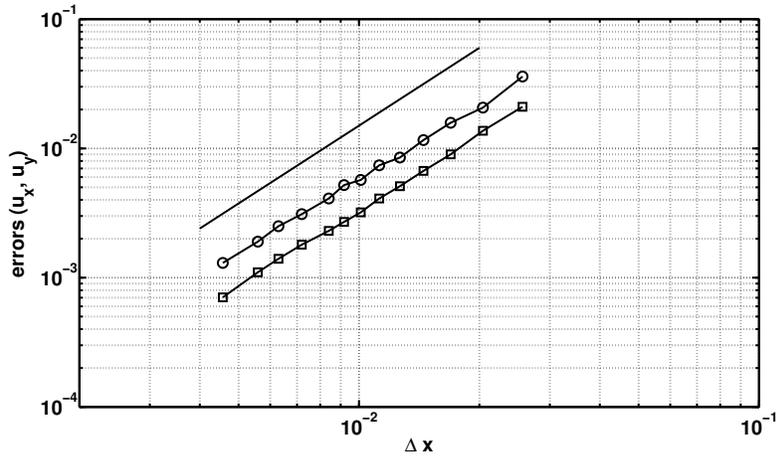
Figure 12: (Flow on an irregular domain example). Convergence plots for the partial derivatives of the horizontal velocity: u_y (circles: ∘) and u_x (squares: □). The errors (in the L^∞ norm) are computed at the fixed time $t = 0.0657$, for different grid resolutions, with $\Delta t = 0.2\,(\Delta x)^2$. The slope of the solid straight line corresponds to the second order scaling error $\propto (\Delta x)^2$. The fact that the errors for the gradient of the velocity are also second order is important — see § 7.4.
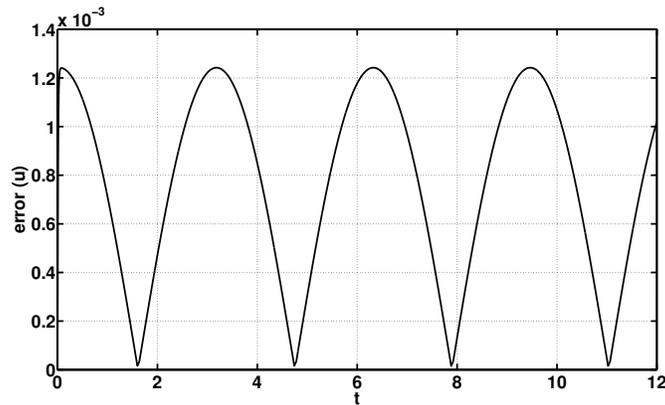
Figure 13: (Flow on an irregular domain example, on an 80×80 grid). Evolution in time of the L^∞ norm of the (spatial) error for the horizontal velocity.

gradient of the velocity is also second order accurate — see figure 12 and remark 12, a feature that should be particularly useful for the calculation of fluid-solid forces (stresses) along domain boundaries.
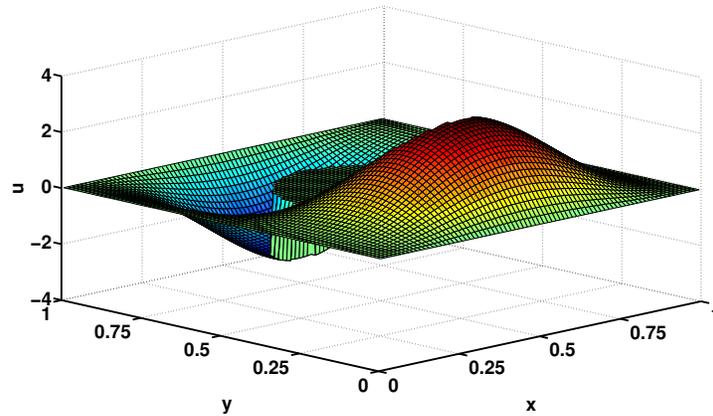

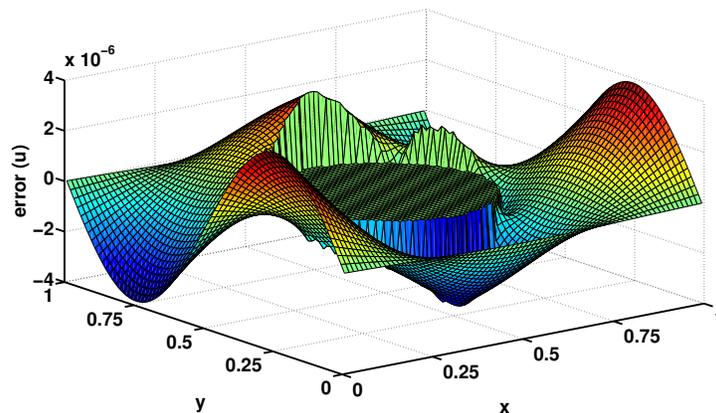Figure 14: (Flow on an irregular domain example, on an 80×80 grid). Numerical horizontal velocity field u at $t = 4\pi$.

Figure 15: (Flow on an irregular domain example, on an 80×80 grid). Error field for the horizontal velocity u at $t = 4\pi$.

Similarly, figure 16 shows plots of the pressure and of the associated pressure error field, again for the time $t = 4\pi$. Just as in the case of the

43

velocity, the errors are dominated at the boundary. We did not check the order of convergence for the gradient of the pressure since one does not need the gradient of the pressure to compute forces.
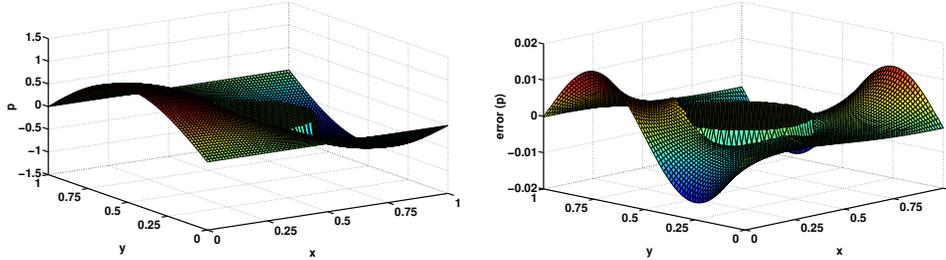

Figure 16: (Flow on an irregular domain example, on an 80×80 grid). Left: numerical pressure field p at $t = 4\pi$. Right: associated error field.

Finally, figure 17 shows a plot of the error in the numerical divergence of the flow field, also for time $t = 4\pi$. The errors in the divergence are also second order. However: notice that they are much smaller than the errors in the flow field or in the pressure. This is indicative of the rather strong enforcement of incompressibility that equations (9) and (10) guarantee.
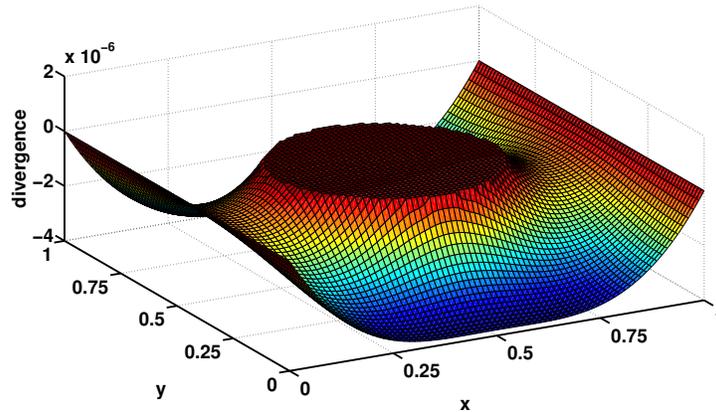

Figure 17: (Flow on an irregular domain example, on an 80×80 grid). Numerical error in the divergence of the velocity at $t = 4\pi$. The $O(10^{-6})$ amplitude is the result of the $O(\Delta x^2)$ order of the scheme.

44

7.4. Convergence of the derivatives

A key reason to worry about uniform convergence, up to the boundary, of the numerical solution is that this is a necessary condition for the accurate modeling of solid-fluid interactions. The evaluation of fluid-solid stresses requires both the pressure, as well as the derivatives of the velocities, to be accurate at the boundaries. Hence, in this paper we investigated the behavior of the errors for not just the pressure p and the velocity fields (u, v), but for the gradient of the flow velocity as well.

An *important point* to notice is that figure 12 shows that

$$\left.\begin{array}{c} \text{The derivatives of the velocities exhibit errors that} \\ \text{appear to be second order as well— in the } L^\infty \text{ norm.} \end{array}\right\} \qquad (77)$$

At first sight this may seem surprising: since the velocities are second order accurate, one would expect their derivatives to be first order only. However, this is a worse case scenario, based on the assumption of random errors. On the other hand, the errors for finite differences approximations (on regular grids) are typically *not* random: If the solutions are smooth enough, the errors can be expanded in powers of Δx, with coefficients that involve derivatives of the solution. Hence, in this case, taking low order derivatives[13] does not degrade the order of convergence. This, of course, is an important advantage of finite differences over other approaches (e.g. projection) which do not have this property.

The astute reader may have noticed that the argument in the prior paragraph avoids the issue of boundary condition implementation, which can ruin the smooth error expansions available for finite differences. This requires some extra considerations:

7a On conforming boundaries, it is usually possible to approximate the boundary conditions in such a way that smooth expansions (in powers of Δx) remain available for the truncation errors.

7b On non-conforming boundaries, on the other hand, it is very easy to ruin the smooth error expansions. The local stencils used to approximate the boundary conditions along the boundary will, typically, experience abrupt changes in response to the placement of the boundary relative to the regular grid.

---

[13]At high order, round off errors dominate. There is an irreducible $O(\epsilon (\Delta x)^{-q})$ contribution from them, where ϵ is the round off error, and q is the order of the derivative.

This is where the global approach that we used in § 5.2 to implement the boundary conditions comes to the rescue: by linking each local stencil to its neighbors, the non-smoothness caused by abrupt stencil changes is smeared. Thus a better behaved error is obtained, which then explains why the result in (77) occurs. Notice that, as of now, we neither know if the smearing process is enough to make the errors C^1 at leading order — which is what is needed to make the errors in the velocity gradient second order, nor if the errors in the velocity gradient are actually second order. However, the numerical evidence seems to point in this direction.

A final point is that, the "simplest" way to get around the issue in item 7b above, is to implement the boundary conditions at a higher order than required. This has the disadvantage that it can lead to a messier than needed algorithm, but (generally) it should not significantly increase the computational cost — since it only involves the boundary points of the grid.

8. Conclusions

Through the introduction of the pressure Poisson equation with consistent boundary conditions, we give an equivalent formulation of the incompressible Navier-Stokes equations. In this formulation the momentum equation takes the form of a vector heat equation with unconventional boundary conditions, while the pressure Poisson equation can be used to explicitly describe the pressure as a function of velocity at any fixed time. It follows that the reformulated system of equations is ideal for using efficient numerical marching methods, where there are no particular theoretical limitations to the order of accuracy or the method of implementation.

In addition, we devise and implement a second order discretization (uniform up to the boundary) of the equations on irregular domains. We address the issue of numerical stability for the normal boundary velocity by adding an appropriate feedback term to the equations. For the scheme, we use finite differences on a regular, staggered grid, so that the domain boundary can be immersed within an $N \times M$ mesh. We discretize to second order spatial accuracy, and verify the order of accuracy in L^∞, both for the velocity and the pressure on an irregular domain. Hence, the solutions[14] converge $O((\Delta x)^2)$ uniformly (all the way up to the boundary) as the grid spacing $\Delta x \to 0$.

---

[14]Note that we have explored only the case where the solution is at least C^4.

Although, we formulate and implement the scheme in two dimensions, the algorithm has a natural extension to three dimensions.

There are several issues and extensions that we hope to address in future work. First, for irregular domains on a regular grid, the proposed momentum equation boundary conditions implicitly couple all the components of the velocity field. Therefore, the resulting vector heat operator, $\partial_t - \mu \Delta$, cannot be solved "component by component". This makes the implementation of schemes that do a naive implicit treatment of the stiff viscosity term computationally expensive, is there a better way? Second, the formulation in this paper is for fixed domains, but extensions to deformable and or moving geometries seem possible. Third, can the ideas in this paper be extended to flows with variable densities (e.g.: stratified flows)? Lastly, there is the issue of obtaining implementation of the boundary conditions that yield smooth errors. As explained in § 7.4, this guarantees that the derivatives of the flow velocity have the same order of accuracy as the velocity itself, allowing an accurate calculation of the fluid forces on objects immersed in the flow (as well as the domain boundaries).

Acknowledgments

Appendix A. Further Modification for Solvability

In this appendix we address the question posed and motivated in remark 7. Namely: *Can the equations in (20–21) be modified in such a way that they make sense even for initial conditions that are not incompressible?* In fact, in such a way that if a solution starts with $\nabla \cdot \mathbf{u} \neq 0$ and $\mathbf{n} \cdot (\mathbf{u} - \mathbf{g}) \neq 0$, then (as $t \to \infty$) $\nabla \cdot \mathbf{u} \to 0$ and $\mathbf{n} \cdot (\mathbf{u} - \mathbf{g}) \to 0$ — so that the solution converges towards a solution of the Navier-Stokes equation.

As pointed out in remark 7, the problem with (20–21) is that the solvability condition for the Poisson equation (21) is not satisfied when $\nabla \cdot \mathbf{u} \neq 0$. Hence the equations become ill-posed, as they have no solution. The obvious answer to this dilemma is to interpret the solution to (21) in an appropriate least squares sense, which is equivalent to modifying the non-homogeneous terms in the equation by *projecting* them onto the space of right hand sides for which the Poisson equation has a solution. Symbolically, write (21) in the form

$$\left. \begin{array}{rcll} \Delta p & = & g & \text{for } \mathbf{x} \in \ \Omega, \\ \mathbf{n} \cdot \nabla p & = & h & \text{for } \mathbf{x} \in \partial\Omega, \end{array} \right\} \tag{A.1}$$

where g and h are defined in (21). Then modify the equation to

$$\left. \begin{array}{rcll} \Delta p & = & g_p & \text{for } \mathbf{x} \in \ \Omega, \\ \mathbf{n} \cdot \nabla p & = & h_p & \text{for } \mathbf{x} \in \partial\Omega, \end{array} \right\} \tag{A.2}$$

where $(g_p, \, h_p) = \mathbb{P}\,(g, \, h)$ for some projection operator $\mathbb{P}$ such that

$$\int_\Omega g_p \ \mathrm{d}V = \int_{\partial\Omega} h_p \ \mathrm{d}A. \tag{A.3}$$

The question, however, is: which projection?

The discretization failures in solvability arising during the course of a numerical calculation are small, since it should be $(g_e, \, h_e) - (g, \, h) = O\left((\Delta x)^q\right)$ — where q is the order of the method, and $(g_e, \, h_e)$ is the exact right hand side. Thus one can argue that, as long as $(g_p, \, h_p) - (g, \, h) = O((\Delta x)^q)$, the resulting numerical solution will be accurate to within the appropriate order — see remarks 7 and 11. In this section, however, the aim is to consider situations where there is no small parameter (i.e. Δx) guaranteeing that solvability is "almost" satisfied. In particular, we want to consider situations where $\nabla \cdot \mathbf{u} \neq 0$, and $|\nabla \cdot \mathbf{u}| \ll 1$ does not apply — leading to errors in solvability which are not small. It follows that here we must be careful with the choice of the projection.

Obviously, a very desirable property of the selected projection is that it should preserve the validity of equations (9–10) — so that the time evolution drives $\nabla \cdot \mathbf{u}$ to zero. Hence: *it must be that $g_p = g$, with only h affected by the projection*. Further: since the solvability condition involves h only via its mean value over $\partial\Omega$, the simplest projection that works is one that appropriately adjusts the mean of h, and nothing else. Thus we propose to

modify the equations in (20–21) as follows: leave (20) as is, as well as the imposed boundary condition constraint (4), but replace (21) by

$$
\left.
\begin{aligned}
\Delta p &= -\nabla \cdot ((\mathbf{u} \cdot \nabla)\,\mathbf{u}) + \nabla \cdot \mathbf{f} && \text{for } \mathbf{x} \in \ \Omega, \\
\mathbf{n} \cdot \nabla p &= \mathbf{n} \cdot (\mathbf{f} - \mathbf{g}_t + \mu\,\Delta\,\mathbf{u} - (\mathbf{u} \cdot \nabla)\,\mathbf{u}) \\
&+ \ \lambda\,\mathbf{n} \cdot (\mathbf{u} - \mathbf{g}) - \mathcal{C} && \text{for } \mathbf{x} \in \partial\Omega,
\end{aligned}
\right\}
\qquad (\text{A.4})
$$

where

$$
\mathcal{C} = \frac{1}{S} \int_{\partial\Omega} \mathbf{n} \cdot (\mu\,\Delta\,\mathbf{u} + \lambda\,\mathbf{u}) \ \mathrm{d}\,A, \qquad (\text{A.5})
$$

and $S = \int_{\partial\Omega} \mathrm{d}\,A$ is the surface area of the boundary. In terms of (A.1–A.2) this corresponds to the projection

$$
g_p = g \quad \text{and} \quad h_p = h - \mathcal{C}, \qquad (\text{A.6})
$$

where

$$
\mathcal{C} = \frac{1}{S} \left(\int_{\partial\Omega} h \ \mathrm{d}\,A - \int_{\Omega} g \ \mathrm{d}\,V \right). \qquad (\text{A.7})
$$

This is clearly a projection, since $\mathcal{C} = 0$ for $(g_p,\ h_p)$, so that $\mathbb{P}^2 = \mathbb{P}$. Further, since the solvability condition for (A.1) is precisely $\mathcal{C} = 0$ — see equation (A.3), the solvability condition for (A.4) is satisfied — even if $\nabla \cdot \mathbf{u} \neq 0$, though (of course) $\mathcal{C} = 0$ when $\nabla \cdot \mathbf{u} = 0$.

Finally, we remark (again) that the projection in (A.6) is not unique. In particular, numerical implementations of the Poisson equation with Neumann conditions often use least squares projections, which alter both the boundary condition h and the source term g. This makes sense if the solvability errors are small. However, in general it seems desirable to not alter the source term, and keep (9–10) valid. This still does not make (A.6) unique, but it makes it the simplest projection. Others would also alter (in some appropriate eigenfunction representation) the zero mean components of h. This seems not only un-necessarily complicated, but it may also affect the validity of the result stated below equation (A.8), defeating the whole purpose of the reformulation in this appendix.

The system of equations in (20) and (A.4) makes sense for arbitrary flows $\mathbf{u}$, which are neither restricted by the incompressibility condition $\phi = \nabla \cdot \mathbf{u} = 0$ in Ω, nor the normal velocity boundary condition $\mathcal{E} = \mathbf{n} \cdot (\mathbf{u} - \mathbf{g}) = 0$. Furthermore: *this system, at least in bounded domains Ω, includes the Navier-Stokes equations as a global attractor for the smooth solutions.* This is easy to see as follows:

First, because of equations (9–10), ϕ decays exponentially, at a rate controlled by the smallest eigenvalue of $L = -\Delta$ in Ω, with Dirichlet boundary conditions. In particular:

$$\mathcal{C} = \frac{1}{S} \int_{\partial\Omega} \mathbf{n} \cdot (\mu \, \Delta \, \mathbf{u} + \lambda \, \mathbf{u}) \; \mathrm{d} A = \frac{1}{S} \int_{\Omega} (\mu \, \Delta \, \phi + \lambda \, \phi) \; \mathrm{d} V$$

vanishes exponentially.

Second, it is easy to see that, for the system in (20) and (A.4), equation (22) is modified to

$$\mathcal{E}_t = -\lambda \, \mathcal{E} + \mathcal{C} \quad \text{for} \;\; \mathbf{x} \in \partial\Omega, \tag{A.8}$$

where $\mathcal{E} = \mathbf{n} \cdot (\mathbf{u} - \mathbf{g})$. Hence $\mathcal{E}$ also vanishes exponentially.

Of course, if $\phi = 0$ and $\mathcal{E} = 0$ initially, then they remain so for all times, and the evolution provided by (20) and (A.4) is, exactly, the Navier-Stokes evolution.

In conclusion, the formulation in this section is not only an interesting theoretical fact. It also provides a robust framework within which numerical solvers for the incompressible Navier Stokes equations can be developed, without having to worry about the (potentially deleterious) effects that discretization (or initial condition) errors, can cause when they violate mass conservation — because either $\nabla \cdot \mathbf{u} = 0$ in Ω, or $\mathbf{n} \cdot (\mathbf{u} - \mathbf{g}) = 0$ in $\partial\Omega$, fail. In addition, the formulation eliminates the necessity of having to enforce the condition $\nabla \cdot \mathbf{u} = 0$ directly, which is a core difficulty for the solution of the Navier-Stokes equations.

Appendix B. The $\nabla \cdot \mathbf{u} = 0$ Boundary Condition

In the main body of the paper, the $\nabla \cdot \mathbf{u} = 0$ boundary condition is implemented using a regular Cartesian grid. In Cartesian coordinates, this boundary condition relates the horizontal and vertical velocities (for two dimensions) via the standard formulas

$$\mathbf{u} = u \, \hat{\boldsymbol{\imath}} + v \, \hat{\boldsymbol{\jmath}}, \tag{B.1}$$

$$\nabla \cdot \mathbf{u} = \frac{\partial u}{\partial x} + \frac{\partial v}{\partial y}, \tag{B.2}$$

where $\hat{\boldsymbol{\imath}}$ and $\hat{\boldsymbol{\jmath}}$ are the coordinate unit vectors.

For some applications, it may be more convenient to implement the numerical computation on a coordinate system where the boundaries are conforming. In general curvilinear coordinate systems, the divergence acquires a more complicated form than the one above. Hence, it is our purpose here to display the form that the $\nabla \cdot \mathbf{u} = 0$ boundary condition takes for a conforming boundary in a general orthogonal curvilinear coordinate system. We do the 2-D case only — the 3-D case is quite similar.

Appendix B.1. Curvilinear coordinates and a conforming boundary

In some region near the boundary $\partial \Omega$ of the domain of integration, assume that an orthogonal, curvilinear, set of coordinates (η, ξ) has been selected — such that the boundary is given by $\eta = c$, for some constant c. In terms of the coordinates (η, ξ), the vector field $\mathbf{u}$ can then be written in the form

$$\mathbf{u} = u_\eta \, \hat{\boldsymbol{\eta}} + u_\xi \, \hat{\boldsymbol{\xi}}, \tag{B.3}$$

where u_η and u_ξ are the velocity components in the coordinate directions given by the unit vectors $\hat{\boldsymbol{\eta}}$ and $\hat{\boldsymbol{\xi}}$, respectively. Let now the functions $x = x(\eta, \xi)$ and $y = y(\eta, \xi)$ describe the relationship of the curvilinear coordinates with a Cartesian system. Then (e.g. see [22])

$$\hat{\boldsymbol{\eta}} = \frac{1}{s_\eta} \left(\frac{\partial x}{\partial \eta} \, \hat{\boldsymbol{\imath}} + \frac{\partial y}{\partial \eta} \, \hat{\boldsymbol{\jmath}} \right) \quad \text{and} \quad \hat{\boldsymbol{\xi}} = \frac{1}{s_\xi} \left(\frac{\partial x}{\partial \xi} \, \hat{\boldsymbol{\imath}} + \frac{\partial y}{\partial \xi} \, \hat{\boldsymbol{\jmath}} \right), \tag{B.4}$$

where s_η and s_ξ are local normalization factors

$$s_\eta^2 = \left(\frac{\partial x}{\partial \eta} \right)^2 + \left(\frac{\partial y}{\partial \eta} \right)^2 \quad \text{and} \quad s_\xi^2 = \left(\frac{\partial x}{\partial \xi} \right)^2 + \left(\frac{\partial y}{\partial \xi} \right)^2. \tag{B.5}$$

Further, re-interpreting s_η and s_ξ as functions of (η, ξ), we have

$$\nabla \cdot \mathbf{u} = \frac{1}{s_\eta \, s_\xi} \left(\frac{\partial}{\partial \eta} (s_\xi \, u_\eta) + \frac{\partial}{\partial \xi} (s_\eta \, u_\xi) \right). \tag{B.6}$$

The $\nabla \cdot \mathbf{u} = 0$ boundary condition is accompanied by the Dirichlet boundary condition $\mathbf{n} \times \mathbf{u} = \mathbf{n} \times \mathbf{g}$ for the vector momentum equation. For a conforming boundary, this is just $u_\xi = g_\xi$ along the boundary curve where $\eta = c$. Thus the $\nabla \cdot \mathbf{u} = 0$ boundary condition reduces to a *Robin* boundary condition on the normal velocity (provided that the boundary is piecewise smooth)

$$\frac{\partial}{\partial \eta} (s_\xi \, u_\eta) + \frac{\partial}{\partial \xi} (s_\eta \, g_\xi) = 0 \tag{B.7}$$

along $\eta = c$.

Appendix B.2. Example: polar coordinates

Consider the special case of a polar coordinate system $x = r\cos\theta$ and $y = r\sin\theta$, with the boundary at $r = 1$. Let the angular velocity at the boundary be given by $u_\theta(1, \theta) = g_\theta(\theta)$. Then since (in this case) $s_\theta = r$ and $s_r = 1$, the zero divergence boundary condition becomes

$$\frac{\partial}{\partial r}(r\,u_r) + \frac{\partial}{\partial\theta}\,g_\theta = 0 \quad \text{for} \ \ r = 1. \tag{B.8}$$

References

[1] P. Angot, C.-H. Bruneau, P. Fabrie, *A penalization method to take into account obstacles in viscous flows,* Numerische Mathematik, **81** (1999) 497-520.

[2] J. B. Bell, P. Collela, H. M. Glaz, *A second-order projection method for the incompressible Navier-Stokes equations,* J. Comput. Phys. **85** (1989) 257-283.

[3] M. Ben-Artzi, J.-P. Croisille, D. Fishelov, S. Trachtenberg, *A pure-compact scheme for the streamfunction formulation of the Navier-Stokes equations,* J. Comput. Phys. **205** (2005) 640-644.

[4] D. L. Brown, R. Cortez, M. L. Minion, *Accurate projection methods for the incompressible Navier–Stokes equations,* J. Comput. Phys. **168** (2001) 464-499.

[5] D. Calhoun, *A Cartesian grid method for solving the two-dimensional stream function-vorticity equations in irregular regions,* J. Comput. Phys. **176** (2002) 231-275.

[6] C. Canuto, M. Y. Hussaini, A. Quarteroni, T. A. Zang, *Spectral Methods: Evolution to Complex Geometries and Applications to Fluid Dynamics,* Springer-Verlag, Berlin Heidelberg, 2007.

[7] A. J. Chorin, *Numerical solutions of the Navier-Stokes equations,* Math. Comput. **22** (1968) 745-762.

[8] W. E, J.-G. Liu, *Gauge method for viscous incompressible flows*, Commun. Math. Sci. 1 (2003) 317332.

[9] J. Ferziger, M. Peric, *Computational Methods for Fluid Dynamics,* Third Edn., Springer-Verlag, New York, (2002) 76-81.

[10] U. Ghia, K. N. Ghia, C. T. Shin, *High-Re Solutions for incompressible flow using the Navier-Stokes Equations and a multigrid method*, J. Comput. Phys. **48** (1982) 387-411.

[11] R. Glowinski, T.-W. Pan, A. J. Kearsley, J. Periaux, *Numerical simulation and optimal shape for viscous flow by a fictitious domain method,* Int. J. Numer. Meth. Fluids **20** (1995) 695-711.

[12] D. Goldstein, R. Handler, L. Serovich, *Modeling a no-slip flow boundary with an external force field,* J. Comput. Phys. **105** (1993) 354-366.

[13] D. Gottlieb, S. Orzag, *Numerical Analysis of Spectral Methods: Theory and Applications,* SIAM, Philadelphia, 1977.

[14] D. Greenspan, *Introduction to Numerical Analysis of Elliptic Value Problems,* Int. Edn., Harper New York, (1965) 39-42.

[15] P. M. Gresho, R. L. Sani, *On presssure boundary conditions for the incompressible Navier-Stokes equations,* Int. J. Numer. Methods Fluids **7** (1987) 1111-1145.

[16] J. L. Guermond, P. Minev, Jie Shen, *An Overview of projection methods for incompressible flows,* Comput. Methods in Appl. Mech. Eng. **195** (2006) 6011-6045.

[17] A. Hammouti, *Simulation Numérique Directe en différence finie de l'écoulement d'un fluide incompressible en présence d'une interface rigide,* docteur és sciences theses, December 2009, Ecole Nationale des Ponts et Chaussés, Paris, France.

[18] F. H. Harlow, J. E. Welch, *Numerical calculation of time-dependent viscous incompressible flow of fluid with free surface,* Phys. Fluids **8** (1965) 2182-2189.

[19] W. D. Henshaw, *A Fourth-Order Accurate Method for the Incompressible Navier-Stokes Equations on Overlapping Grids,* J. Comput. Phys. **113** (1994) 13-25.

[20] W. D. Henshaw, H.-O. Kreiss, L. G. M. Reyna, *A Fourth-Order Accurate Difference Approximation for the Incompressible Navier-Stokes Equations*, J. Comput. Fluids **23** (1994) 575-593.

[21] W. D. Henshaw, N. Anders Petersson, *A Split-Step Scheme for the Incompressible Navier-Stokes Equations*, (Numerical Simulation of Incompressible Flows, World Scientific, editor M.M. Hafez), (2003) 108-125.

[22] T. A. S. Jackson, *Orthogonal Curvilinear Coordinates,* The Mathematical Gazette, **50**, 371 (1966) 28-30.

[23] H. Johnston, J.-G. Liu, *A finite difference method for incompressible flow based on local pressure boundary conditions,* J. Comput. Phys. **180** (2002) 120-154.

[24] H. Johnston, J.-G. Liu, *Accurate, stable and efficient Navier-Stokes solvers based on explicit treatment of the pressure term,* J. Comput. Phys. **199** (2004) 221-259.

[25] G. Karniadakis, M. Israeli, S. A. Orszag, *High-order splitting methods for the incompressible Navier-Stokes equations,* J. Comput. Phys. **97** (1991) 414-443.

[26] K. Khadra, P. Angot, S. Parneix, J.-P. Caltagirone, *Fictitious domain approach for numerical modelling of Navier-Stokes equations,* Int. J. Numer. Meth. Fluids **34** (2000) 651-684.

[27] J. Kim, P. Moin, *Application of a fractional step method to incompressible Navier-Stokes equations,* J. Comput. Phys. **59** (1985) 308-323.

[28] L. Kleiser, U. Schumann, *Treatment of the incompressibility and boundary conditions in 3-D numerical spectral simulation of plane channel flows,* in E. H. Hirschel (Ed.), Notes on Numerical Fluid Mechanics, Vieweg, Braunschweig, 1980, pp. 165-173.

[29] A. Krzywicki, O. A. Ladyzhenskaya, *A grid method for the Navier-Stokes equations,* Dokl. Akad. Nauk SSSR **167** (1966) 309-311. English transl., Soviet Physics Dokl. **11** (1966) 212-213.

[30] P. D. Lax, R. D. Richtmyer, *Survey of the stability of linear finite difference equations*, Comm. Pure Appl. Math. **9** (1956) 267-293.

[31] M. Linnick, H. Fasel, *A high-order immersed interface method for simulating unsteady incompressible flows on irregular domains,* J. Comput. Phys. **204** (2005) 157-192.

[32] J.-G. Liu, J. Liu, R. Pego, *Stable and accurate pressure approximation for unsteady incompressible viscous flow,* J. Comput. Phys., **229** (2010) 3428-3453.

[33] R. Mittal, G. Iaccarino, *Immersed boundary methods,* Ann. Rev. Fluid Mech. **37** (2005) 39-261.

[34] M. Napolitano, G. Pascazio, L. Quartapelle, *A review of vorticity conditions in the numerical solution of the $\zeta - \psi$ equations,* J. Comput. Fluids **28** (1999) 139-185.

[35] S. A. Orszag, M. Israeli, M. Deville, *Boundary conditions for incompressible flows,* J. Sci. Comput. **1** (1986) 75-111.

[36] J. B. Perot, *An analysis of the fractional step method,* J. Comput. Phys. **108** (1993) 51-58.

[37] C. S. Peskin, *Flow patterns around heart valves: a numerical method,* J. Comput. Phys. **10** (1972) 252-271.

[38] C. S. Peskin, *The immersed boundary method,* Acta Numerica **11** (2002) 479-517

[39] N. A. Petersson, *Stability of Pressure Boundary Conditions for Stokes and Navier-Stokes Equations*, J. Comput. Phys. **172** (2001) 40-70.

[40] A. Prohl, *Projection and quasi-compressibility methods for solving the incompressible Navier-Stokes equations,* Advances in Numerical Mathematics, Wiley-Teubner series, advances in numerical mathematics, B.G. Teubner, Stuttgart, 1997.

[41] L. Quartapelle, *Numerical Solution of the Incompressible Navier-Stokes Equations,* Birkhauser Verlag, 1993.

[42] R. Rannacher, *On Chorin's projection method for the incompressible Navier-Stokes equations,* in: Lecture Notes in Mathematics, **1530** (1991) 167-183.

[43] D. Rempfer, *On Boundary conditions for the incompressible Navier-Stokes problems,* Applied Mechanics Reviews **59** (2006) 107-125.

[44] R. Sani, J. Shen, O. Pironneau, P. Gresho, *Pressure boundary condition for the time-dependent incompressible Navier-Stokes equations,* Int. J. Numer. Methods Fluids **50** (2006) 673-682.

[45] J. Shen, *On error estimates of the projection methods for the Navier-Stokes equations: first-order schemes,* SIAM J. Numer. Anal. **29** (1992) 57-77.

[46] J. C. Strikwerda, *Finite Difference Schemes and Partial Differential Equations*, Wadsworth and Brooks Cole (1989).

[47] K. Taira, T. Colonius, *The Immersed boundary method: A projection approach,* J. Comput. Phys. **225** (2007) 2118-2137.

[48] R. Temam, *Sur l'approximation de la solution des equations de Navier-Stokes par la methode des pas fractionnaries, ii,* Arch. Ration. Mech. Anal. **33** (1969) 377-385.

[49] M. Taylor, *Partial differential equations III, Nonlinear equations*, Springer New York, (1996).

[50] J. van Kan, *A second-order accurate pressure-correction scheme for viscous incompressible flow,* SIAM J. Sci. Stat. Comput. **7** (1986) 870-891.